

A Spline-Based Approach to Uncertainty Quantification and Density Estimation

Adi Ditzkowski^a, Gadi Fibich^a, Amir Sagiv^{a,b}

^a*School of Mathematical Sciences, Tel Aviv University, Tel Aviv 6997801, Israel*

^b*corresponding author: asagiv88@gmail.com*

Abstract

In mathematical models with uncertainties and noise, the calculation of a deterministic “quantity of interest” (model output) is often replaced by the calculation of its moments (mean, standard deviation, etc.) and probability density function. Standard methods for these tasks are either statistical (Monte-Carlo, kernel density estimators, etc.) or spectral approximations (e.g., generalized polynomial chaos). In this paper we present a novel spline-based algorithm for these tasks. Our method offers significant advantages over the existing methods for density estimation, including a guaranteed convergence rate which is at least cubic in the number of samples. Furthermore, although spectral methods can approximate moments with exponential accuracy, the spline-based approximation is often more accurate when the sample size is small. We also show how to approximate the moments and density of non-smooth quantities of interest, which is often prohibitive in spectral methods. Finally, we demonstrate our algorithm for problems in nonlinear optics and computational fluid dynamics.

Keywords: Uncertainty Quantification, Density Estimation, Nonlinear Dynamics, Nonlinear PDE, Spline

1. Introduction

Uncertainties and noise are prevalent in mathematical models in all branches of science. In such cases, the solution of the (otherwise deterministic) model becomes random, and so one is interested in computing its statistics. This problem, sometimes known as *forward uncertainty propagation* (UQ), arises in various areas such as biochemistry [1, 2], fluid dynamics [3, 4, 5, 1], structural engineering [6], hydrology [7], and nonlinear optics [8].

In many applications, one is interested in computing the *probability density function* (PDF) of a “quantity of interest” (output) of the model [4, 2, 5, 9, 8]. Since standard forward UQ methods [6, 10] such as Stochastic Finite Element, or generalized Polynomial Chaos (gPC) [11, 12, 13, 14, 15, 16], hp-gPC [17], and Wiener-Haar expansion [18] can approximate moments with spectral accuracy [19, 20], these methods have been used for *density estimation* as well. In this paper, we point out that spectral methods are often a poor choice for this task, and propose a novel *spline-based* method for density estimation. Perhaps surprisingly, this problem received little attention so far, despite its relevance.

Unlike standard UQ methods (such as gPC), our spline-based method can provide a good approximation to the density using a small sample size, and it has a guaranteed convergence rate which is at least cubic. Because we rely only on solving the underlying deterministic model (i.e., our method is non-intrusive), and because interpolation by spline is a standard numerical procedure, our proposed method is easy to implement. Furthermore, both the gPC and spline-based methods can approximate moments and the PDF of some *non-smooth* quantities of interest.

Given only N independently and identically distributed (iid) samples of the quantity of interest, non-parametric statistics methods, such as kernel density estimators [21, 22] are guaranteed to converge as fast as $N^{-1} \log(N)$, which in these settings is optimal [23]. When, however, the deterministic relation between the randomness parameter and the quantity of interest is known and is smooth, both gPC and our spline-based method converge much faster.

In many applications each solution of the deterministic model is computationally expensive, which limits the number of available samples. In these cases, spectrally-convergent methods (such as gPC) might fail to attain the desired accuracy due to insufficient sampling resolution. In contrast, the spline-based method approximates moments accurately even when the sample size is relatively small. In addition, high-derivatives and discontinuities have little effect on our method’s accuracy, due to the fact that spline interpolation is predominantly local (see Sec. 4). Another advantage over gPC is that splines are not limited to a specific choice of sampling points.

The paper is organized as follows. In Sec. 2 we introduce the general settings and notations. Sec. 3 briefly reviews standard statistical methods and the gPC method for moment and density estimation. Sec. 4 presents and analyzes our spline-based algorithm for moments and density estimation. We compare this method to gPC and KDE for an “artificial” toy example (Sec. 5), for the rotation angle of the polarization ellipse in nonlinear optics (Sec. 6), and for the shock location in the Burgers equation (Sec. 7). In all these cases we observe that the spline-based density estimation converges at least at a cubic rate, and the spline-based moments are more accurate than the gPC ones when the sample sizes are small. Sec. 8 concludes with open questions and future research directions.

2. Settings and computational goals

We consider initial value problems of the form

$$u_t(t, \mathbf{x}; \boldsymbol{\alpha}) = Q(u, \mathbf{x}; \boldsymbol{\alpha})u, \quad u(t = 0, \mathbf{x}; \boldsymbol{\alpha}) = u_0(\mathbf{x}; \boldsymbol{\alpha}), \quad (1)$$

where $\mathbf{x} \in \mathbb{R}^d$, Q is a possibly nonlinear differential operator, and $\boldsymbol{\alpha} \in \Omega \subset \mathbb{R}^m$ is a random variable which is distributed according to a continuous weight function $c(\boldsymbol{\alpha})$ such that $\int_{\Omega} c(\boldsymbol{\alpha}) d\boldsymbol{\alpha} = 1$. The randomness of $u(t, \mathbf{x}; \boldsymbol{\alpha})$ is due to the dependence of Q and/or u_0 on $\boldsymbol{\alpha}$.

For a given a *quantity of interest* $f(\boldsymbol{\alpha}) := f(u(t, \mathbf{x}); \boldsymbol{\alpha})$, we may wish to perform:

1. **Moment estimation.** Compute the mean, variance, or standard deviation of $f(\boldsymbol{\alpha})$:

$$\mathbb{E}_{\boldsymbol{\alpha}}[f] := \int_{\Omega} f(\boldsymbol{\alpha}) c(\boldsymbol{\alpha}) d\boldsymbol{\alpha}, \quad \text{Var}[f] := |\mathbb{E}_{\boldsymbol{\alpha}}[f]|^2 - \mathbb{E}_{\boldsymbol{\alpha}}[|f|^2], \quad \sigma(f) := \sqrt{\text{Var}[f]}. \quad (2)$$

2. **Density estimation.** Compute the probability distribution function (PDF) of $f(\boldsymbol{\alpha})$.

$$p(y) := \frac{dP(y)}{dy}, \quad y \in \mathbb{R}, \quad (3a)$$

where P is the cumulative distribution function (CDF),

$$P(y) := \text{Prob}\{f(\boldsymbol{\alpha}) < y\}. \quad (3b)$$

2.1. Applications

Some examples of these general settings are:

1. **Effect of shot-to-shot variation in nonlinear optics**, see Sec. 6.
2. **Hydrodynamical shock formation**, see Sec. 7.
3. **Out-of-equilibrium chemical reactions.** Belosouov-Zhabotinsky type systems model out-of-equilibrium chemical reactions. One concrete system is the Oregonator [24]

$$\begin{aligned} \frac{dX}{dt} &= k_1 Y - k_2 XY + k_3 X - k_4 X^2, \\ \frac{dY}{dt} &= -k_1 Y - k_2 XY + k_5 Z, \\ \frac{dZ}{dt} &= k_3 X - k_5 Z, \end{aligned}$$

where X , Y , and Z are the concentrations of three different chemical species, and $\{k_i\}_{i=1}^5$ are the rate-parameters, often estimated empirically [1]. For large values of t , this system exhibits sustained, temporal oscillations with a frequency $F = F(k_1, \dots, k_5)$. To deal with an uncertainty in the parameters k_4 and k_5 , the authors of [2] computed the moments of X, Y, Z , and the PDF of the oscillations frequency F . This is an example of (1)–(3) with $\boldsymbol{\alpha} = (k_4, k_5)$ and $f = X, Y, Z$ and F .

4. **Heat convection.** Consider the flow of a fluid in a two-dimensional box $\mathbf{x} = (x, y) \in [x_1, x_2] \times [y_1, y_2]$, which is modeled by the Navier-Stokes like equations

$$\nabla \cdot \mathbf{u} = 0, \quad \frac{\partial \theta}{\partial t} + \mathbf{u} \cdot \nabla \theta = \nabla^2 \theta,$$

$$\frac{\partial \mathbf{u}}{\partial t} + \mathbf{u} \cdot \nabla \mathbf{u} = -\nabla p + \text{Pr} \nabla^2 \mathbf{u} + F(\mathbf{u}, \theta),$$

where $\mathbf{u}(t, \mathbf{x}; \boldsymbol{\alpha})$ is the fluid velocity, $p(t, \mathbf{x}; \boldsymbol{\alpha})$ is the pressure, $\theta(t, \mathbf{x}; \boldsymbol{\alpha})$ is the temperature, Pr is the Prandtl number, and F is the buoyant force [5]. The temperature is a

known constant θ_0 on one side of the box, but is random on the other side, i.e.,

$$\theta(t, x_1, y) \equiv \theta_0, \quad \theta(t, x_2, y) = \theta_1(y; \boldsymbol{\alpha}).$$

The PDF of the pressure and of the velocity were computed in [9] when $\theta_1(y; \alpha) = \theta_1(\alpha)$ and α is uniformly distributed in $[\alpha_{\min}, \alpha_{\max}]$, and in [5] when $\theta_1(y; \boldsymbol{\alpha})$ is a Gaussian random process.

3. Review of existing methods

We briefly present the standard methods in the literature for (1)–(3).

3.1. Monte-Carlo method, the histogram method, and Kernel Density Estimators

Given N independently and identically distributed (iid) samples $\{\boldsymbol{\alpha}_j\}_{j=1}^N$, the simplest moment estimator is the Monte-Carlo approximation $E_{\boldsymbol{\alpha}}[f] \approx \frac{1}{N} \sum_{n=1}^N f(\boldsymbol{\alpha}_n)$. The Monte Carlo method is intuitive and easy to implement. The main drawback of this method is its slow $O(1/\sqrt{N})$ convergence rate. In cases where each computation of $f(\boldsymbol{\alpha}_j)$ is expensive (e.g., when it requires to solve numerically (1) with $\boldsymbol{\alpha} = \boldsymbol{\alpha}_j$), this slow convergence rate can make the Monte-Carlo method impractical.

Density estimation using N iid samples of $f(\boldsymbol{\alpha})$, denoted by $\{f_j\}_{j=1}^N$, is a fundamental problem in non-parametric statistics. A widely-used method for density estimation is the histogram method, in which one partitions the range of $f(\boldsymbol{\alpha})$ into L disjoint bins $\{B_\ell\}_{\ell=1}^L$, and approximates the PDF p with the *histogram estimator*

$$p_{\text{hist}}(y) := \frac{1}{N} \sum_{\ell=1}^L (\# \text{ of samples for which } f_j \in B_\ell) \cdot \mathbb{1}_{B_\ell}(y), \quad (4)$$

where $\mathbb{1}_{B_\ell}$ is the characteristic function of bin B_ℓ [22]. An alternative approach (which, unlike the histogram method, can provide a smooth PDF) is the Kernel Density Estimator (KDE)

$$p_{\text{kde}}(y) := \frac{1}{Nh} \sum_{j=1}^N K\left(\frac{y - f_j}{h}\right), \quad (5)$$

where $h > 0$ is the “window size” and K is the kernel function (e.g., $K(t) = \frac{1}{\sqrt{2\pi}} e^{-\frac{t^2}{2}}$), see [21, 22, 23].

The mean integrated squared errors (MISE)¹ of the histogram method and of KDE (under some mild assumptions), decay no faster than $N^{-\frac{2}{3}}$ and N^{-1} , respectively [22, 23]. As with the Monte-Carlo method, these rates can be too slow when each evaluation of f_j is computationally expensive.

¹MISE is the expectancy of the squared L^2 error of the PDF. Formally, if p is the exact PDF and \tilde{p} its estimator, define $\text{MISE} := \mathbb{E}\left[\int_{-\infty}^{\infty} (p(y) - \tilde{p}(y))^2 dy\right]$, where the expectation is taken over all sets of N iid samples of f . See [22] for further details.

3.2. Generalized Polynomial Chaos

The Monte-Carlo method, the histogram method, and KDE are all statistical methods, in the sense that they only rely on the sampled values $\{f_j\}_{j=1}^N$. Much more information can be extracted from $\{f_j\}_{j=1}^N$ if the two following conditions hold:

1. The “original” $\{\alpha_j\}_{j=1}^N$ for which $f(\alpha_j) = f_j$ are known.
2. $f(\alpha)$ is smooth.²

These two conditions often hold in the general settings of Sec. 2. In such cases, a powerful numerical approach, known as generalized Polynomial Chaos (gPC), can be applied [12, 15, 16, 10].

For clarity, we review the gPC method for a one-dimensional random variable α , i.e., $\Omega \subseteq \mathbb{R}$. We define the set of orthogonal polynomials $\{p_n(x)\}_{n=0}^\infty$ with respect to $c(\alpha)$ by the conditions [25]

$$\text{Deg}(p_n) = n, \quad \int_{\Omega} p_n(\alpha) p_m^*(\alpha) c(\alpha) d\alpha = \delta_{n,m}. \quad (6)$$

This family of orthogonal polynomials constitutes an orthonormal basis of the space of square integrable functions, i.e., for all $f \in L^2(\Omega, c)$,

$$f(\alpha) = \sum_{n=0}^{\infty} \hat{f}(n) p_n(\alpha), \quad \hat{f}(n) := \int_{\Omega} f(\alpha) p_n(\alpha) c(\alpha) d\alpha, \quad n = 0, 1, \dots \quad (7)$$

This expansion *converges spectrally* for the classical families of orthogonal polynomials, e.g., the Hermite and Legendre polynomials.³ Specifically, if f is analytic, the truncated expansion (7) has the exponential accuracy

$$\left\| f(\alpha) - \sum_{n=0}^{N-1} \hat{f}(n) p_n(\alpha) \right\|_2 \sim C e^{-\gamma N}, \quad N \gg 1, \quad (8)$$

for some constants $C, \gamma > 0$ [15, 26, 27].

The expansion coefficients $\{\hat{f}(n)\}$, see (7), can be approximated using the Gauss quadrature formula $\mathbb{E}_{\alpha}[g] \approx \sum_{j=1}^N g(\alpha_j) w_j$, where $\{\alpha_j\}_{j=1}^N$ are the distinct and real roots of $p_N(\alpha)$, $w_j := \int_{\Omega} l_j(\alpha) d\mu(\alpha)$ are the weights, and $l_j(\alpha)$ are the Lagrange interpolation polynomials with respect to $\{\alpha_j\}_{j=1}^N$ [28], yielding

$$\hat{f}(n) \approx \hat{f}_N(n) := \sum_{j=1}^N f(\alpha_j) p_n(\alpha_j) w_j, \quad n = 0, 1, \dots, N-1. \quad (9)$$

²In Sec. 5.4 we show how our method can be extended to non-smooth functions.

³i.e., if f is in C^r , then $\{\hat{f}(n)\} \leq cn^{-r}$, and if f is analytic, then $|\hat{f}(n)| \leq ce^{-\gamma n}$, for some $c, \gamma > 0$.

The gPC collocation approximation is defined by

$$f_N^{\text{gpc}}(\alpha) := \sum_{n=0}^{N-1} \hat{f}_N(n) p_n(\alpha), \quad (10)$$

where $\{\hat{f}_N(n)\}_{n=0}^{N-1}$ are given by (9), see [20].

The difference between moments of two functions f and g is controlled by their L^2 distance:

Lemma 1. *Let (Ω, μ) be a probability space, denote $\|\cdot\|_p := \|\cdot\|_{L^p(\Omega)}$, and let $f, g \in L^2 \cap L^1$. Then*

$$|\mathbb{E}_\alpha[f] - \mathbb{E}_\alpha[g]| \leq \|f - g\|_2, \quad (11a)$$

$$|\text{Var}(f) - \text{Var}(g)| \leq (\sigma(f) + \sigma(g)) \cdot \|f - g\|_2, \quad (11b)$$

$$|\sigma(f) - \sigma(g)| \leq \|f - g\|_2. \quad (11c)$$

Proof. See Appendix A. □

Therefore, we have

Corollary 1. *Let f be analytic, and let f_N^{gpc} be its gPC collocation approximation of order N , see (10). Then the moments (2) of f can be approximated by the respective moments of f_N^{gpc} with exponential accuracy as $N \rightarrow \infty$.*

Proof. Let $g = f_N^{\text{gpc}}$, the collocation gPC approximation of f , see (10). Since f_N^{gpc} converges exponentially to f in the L^2 norm [15, 29], Lemma 1 implies that the moments of f_N^{gpc} converge exponentially to the moments of f . □

For a smooth quantity of interest f , this spectral convergence rate is superior to the Monte-Carlo $1/\sqrt{N}$ convergence rate, which explains the popularity of the gPC collocation method.

In [8] we used the gPC approximation for moments and density estimation:

Algorithm 1 (gPC-based estimation [8]). *Let $\{\alpha_j, w_j\}_{j=1}^N$ be the points and weights of the Gaussian quadrature rule of order N that correspond to the weight function $c(\alpha)$, and let $\{p_n(\alpha)\}_{n=0}^\infty$ be the respective orthogonal polynomials.*

1. For $j = 1, \dots, N$, solve (1) with $\alpha = \alpha_j$ to obtain $u(t, \mathbf{x}; \alpha_j)$.
2. Approximate $u(t, x; \alpha) \approx u_N^{\text{gpc}}(t, \mathbf{x}; \alpha)$, where $u_N^{\text{gpc}}(t, \mathbf{x}; \alpha) := \sum_{n=0}^{N-1} \hat{u}_N(t, \mathbf{x}; n) p_n(\alpha)$ and $\hat{u}_N(u, \mathbf{x}; n) = \sum_{j=1}^N p_n(\alpha_j) u(t, \mathbf{x}; \alpha_j) w_j$ for $n = 0, \dots, N-1$.
3. Approximate $f(\tilde{\alpha}_m) \approx f(u_N^{\text{gpc}}(\cdot, \tilde{\alpha}_m))$ on a sufficiently dense grid $\{\tilde{\alpha}_m\}_{m=1}^M$.

Moment estimation:

4. Use the trapezoidal integration rule with $\{f(\tilde{\alpha}_m)\}_{m=1}^M$ to approximate $\mathbb{E}_\alpha[f]$.⁴

⁴If $f(\alpha)$ is smooth, one can approximate $\mathbb{E}_\alpha = \hat{f}(0) \approx \hat{f}_N(0)$, see [15].

Density estimation:

- 4'. Use the histogram method (4) with $\{f(\tilde{\alpha}_m)\}_{m=1}^M$ to estimate the PDF of f .

Because of its spectral accuracy (Corollary 1), the number of sample points that is required for gPC to achieve a certain precision is considerably smaller than for Monte-Carlo. To the best of our knowledge, however, there is no convergence result for density estimation using gPC which is analogous to Corollary 1.

Algorithm 1 can also approximate *non-smooth* quantities of interest $f(\alpha)$, as long as $u(\cdot; \alpha)$ is smooth, see Sec. 6 and [8]. The choice of the histogram method in step 4 is discussed in Sec. 8.

The evaluation of $\{f(u_N^{\text{gpc}}(\cdot, \tilde{\alpha}_m))\}_{m=1}^M$ in step 3 is computationally cheap, as it amounts to a substitution in a polynomial. Therefore, there is essentially no computational cost for choosing M to be sufficiently high for the histogram method. This algorithm is also non-intrusive, in the sense that it only requires direct simulations of the deterministic system (1) with specific α_j values (as opposed to, e.g., Galerkin-type methods [19, 13, 18]).

4. Spline-based UQ

Despite its many advantages, the gPC-based Algorithm 1 has several drawbacks:

1. The spectral accuracy of the gPC method for moments estimation *does not imply* a similar accuracy for density estimation. Indeed, although the gPC approximation $f_N^{\text{gpc}}(\alpha)$ is frequently used for computing the PDF of $f(\alpha)$, see e.g., [4], it can be very inaccurate for this computational task. Intuitively, this is because the PDF generally depends on $(\frac{df}{d\alpha})^{-1}$, see Lemma 3. Because polynomial approximations tend to be oscillatory, they “add” many artificial extremal points, which produce large deviations from the exact PDF. These oscillations are intrinsic to polynomial interpolation, and tend to further increase as the interpolated data become less smooth.
2. The spectral convergence of the gPC method is attained only *asymptotically* as the number of sample points N becomes sufficiently large. For small or moderate values of N , however, its accuracy may be quite poor, due to insufficient resolution, and the global nature of spectral approximation.
3. The sample points $\{\alpha_j\}_{j=1}^N$ of the gPC method are predetermined by the quadrature rule. Therefore, if one wants to *adaptively* improve the accuracy, one cannot use the samples from the “old” low-resolution grid in the “new” high-accuracy approximation.

To overcome these limitations, we first note that $f_N^{\text{gpc}}(\alpha)$ is an interpolating polynomial of f :

Lemma 2. *The gPC collocation approximation (10) is the interpolating polynomial of f of order $N - 1$ at the Gauss quadrature points $\{\alpha_j\}_{j=1}^N$.*

Proof. See Appendix B. □

This suggests that other interpolants of $f(\alpha)$ can be used in Algorithm 1. In what follows, we argue that for our computational tasks, splines provide a better way to approximate $f(\alpha)$.

We recall that splines are functions that are piecewise polynomial of degree m , with $k < m$ smooth derivatives. Given an interval $\Omega = [\alpha_{\min}, \alpha_{\max}]$ and a grid $\alpha_{\min} = \alpha_1 < \alpha_2 < \dots < \alpha_N = \alpha_{\max}$, the interpolating cubic spline $s_N(\alpha)$ is a C^2 , piecewise-cubic polynomial that interpolates $f(\alpha)$ at $\{\alpha_j\}_{j=1}^N$, endowed with two additional boundary conditions. Three standard choices are:

1. The natural cubic spline, for which $\frac{d}{d\alpha} f_N^{\text{spline}}(\alpha_1) = \frac{d}{d\alpha} f_N^{\text{spline}}(\alpha_N) = 0$.
2. The “not-a-knot” spline, for which $\frac{d^3}{d\alpha^3} f_N^{\text{spline}}$ is continuous at α_2 and α_{N-1} .
3. The clamped spline, for which $\frac{d}{d\alpha} f_N^{\text{spline}}(\alpha_1) = \frac{d}{d\alpha} f(\alpha_j)$ for $j = 1, N$.

Our decision to use splines is motivated by the following reasons:

1. The error of spline interpolation is guaranteed to be “small” for *any* sample size, in the following sense:

Theorem 1 ([30, 31]). *Let $f \in C^4([\alpha_{\min}, \alpha_{\max}])$, and let f_N^{spline} be its “not-a-knot”, clamped or natural cubic spline interpolant. Then*

$$\|(f(\alpha) - f_N^{\text{spline}}(\alpha))^{(m)}\|_{L^\infty[\alpha_{\min}, \alpha_{\max}]} \leq C_{\text{spl}}^{(m)} \|f^{(4)}\|_\infty h_{\max}^{4-m}, \quad m = 0, 1, 2, \quad (12)$$

where $C_{\text{spl}}^{(m)} > 0$ is a universal constant that depends only on the type of boundary condition and m , and $h_{\max} = \max_{1 \leq j \leq N} |\alpha_j - \alpha_{j-1}|$.

2. Spline interpolation is predominantly local. To see this, let us first recall a classical result of Birkhoff and de Boor:

Theorem 2 ([32, 33]). *Let $s_i(\alpha)$ be the natural cubic spline that satisfies $s_i(\alpha_k) = \delta_{i,k}$, where $1 \leq i, k \leq N$ and $\alpha_{\min} = \alpha_1 < \alpha_2 < \dots < \alpha_N = \alpha_{\max}$ is given. Then*

$$\max_{\alpha \notin (\alpha_{i-k}, \alpha_{i+k})} |s_i(\alpha)| \leq A 2^{-k}, \quad 1 < i < N,$$

where $A > 0$ is a constant that depends on the global mesh ratio $\frac{\max_{1 \leq j \leq N} \alpha_j - \alpha_{j-1}}{\min_{1 \leq k \leq N} \alpha_k - \alpha_{k-1}}$.

Therefore, the natural cubic spline $f_N^{\text{spline}}(\alpha)$ is essentially a local approximation:

Corollary 2. *Denote the natural cubic spline $f_N^{\text{spline}} = f_N^{\text{spline}}(\alpha; f_1, \dots, f_N)$ to emphasize the dependence of the spline interpolation on the sampled values. Then*

$$\max_{\alpha \notin (\alpha_{i-k}, \alpha_{i+k})} \left| \frac{\partial f_N^{\text{spline}}(\alpha; f_1, \dots, f_N)}{\partial f_i} \right| \leq A 2^{-k}, \quad 1 < i < N, \quad 1 \leq k \leq N,$$

where $A > 0$ is given by Theorem 2.

Proof. The function $S(\alpha) = \sum_{i=1}^N f_i s_i(\alpha)$, where $s_i(\alpha)$ are defined in Theorem 2, is a C^2 cubic spline, which by definition satisfies $S(\alpha_i) = f_i$, and $\frac{d}{d\alpha}S(\alpha_1) = \frac{d}{d\alpha}S(\alpha_N) = 0$. By the uniqueness of the natural cubic spline, $S(\alpha) = f_N^{\text{gpc}}(\alpha)$, so, $\frac{\partial f_N^{\text{spline}}(\alpha; f_1, \dots, f_N)}{\partial f_i} = s_i(\alpha)$. Hence, by Theorem 2, the corollary is proven. \square

Remark. For a proof of an equivalent result, which is valid also for the “not-a-knot” boundary condition, see Appendix C.

Thus, *although* $f_N^{\text{spline}}(\alpha)$ *depends on* $\{f_1, \dots, f_N\}$, *it predominantly depends on the few values* f_j *for which* α_j *is adjacent to* α . Therefore, large derivatives and discontinuities of $f(\alpha)$ may impair the accuracy of $f_N^{\text{spline}}(\alpha)$ only locally.⁵ This is in contrast to gPC (and polynomial interpolation in general), where discontinuities and large derivatives of f decrease the approximation accuracy across the entire domain.

3. Unlike gPC, splines can be constructed using any choice of sampling points.

In light of these considerations, we propose to replace the gPC interpolant with a spline:

Algorithm 2 (Spline-based estimation). *Let $\{\alpha_j\}_{j=1}^N$ be a uniform grid on $[\alpha_{\min}, \alpha_{\max}]$.*

1. *For $j = 1, \dots, N$, solve (1) with $\alpha = \alpha_j$ to obtain $u(t, \mathbf{x}; \alpha_j)$.*
2. *Approximate $u(t, x; \alpha) \approx u_N^{\text{spline}}(t, \mathbf{x}; \alpha)$, where u_N^{spline} is a cubic spline interpolant on $\alpha_1, \dots, \alpha_N$.*
3. *Approximate $f(\tilde{\alpha}_m) \approx f(u_N^{\text{spline}}(\cdot, \tilde{\alpha}_m))$ on a sufficiently dense grid $\{\tilde{\alpha}_m\}_{m=1}^M$.*

Moment estimation

4. *Use the trapezoidal integration rule with $\{f(\tilde{\alpha}_m)\}_{m=1}^M$ to approximate $\mathbb{E}_\alpha[f]$.*⁶

Density estimation

- 4'. *Use the histogram method (4) with $\{f(\tilde{\alpha}_m)\}_{m=1}^M$ to approximate the PDF of f .*

Remark. See Appendix E for a MATLAB implementation of this algorithm.

Which cubic spline should be used in step 2? If $f'(\alpha_{\min})$ and $f'(\alpha_{\max})$ are known, then one should use the *clamped* cubic spline (or the natural cubic spline if these derivatives are zero). When the boundary derivatives are unknown, however, the “not-a-knot” interpolating cubic spline should be used (as indeed was done in this manuscript). See [34] for further discussion.

Algorithm 2 is *identical* to Algorithm 1, except for two substantial points:

⁵For a review of cubic splines that are *strictly* local, see [34].

⁶When f is sufficiently smooth and α is uniformly distributed, one can approximate $\mathbb{E}_\alpha[f] \approx \mathbb{E}_\alpha[f_N^{\text{spline}}]$, and compute the right-hand side explicitly (in MATLAB, this can be done using the *fnint* command).

1. The sampling grid is uniform, rather than the Gauss quadrature grid.⁷
2. The gPC interpolant u_N^{gpc} is replaced by a cubic spline interpolant u_N^{spline} .

Remark. This method is not to be confused with *spline-smoothing*, in which one approximates the PDF p with splines [35, 36]. Thus, Algorithm 2 approximates u with a spline, but the resulting approximation of the PDF p is *not* a spline.

4.1. Accuracy of spline-based density estimation

The accuracy of the histogram method in step 4' depends on the number of bins L and on the number of samples M at steps 3 and 4'. If the number of bins is chosen to be

$$L_{\text{opt}} = K_f M^{-\frac{1}{3}}, \quad K_f = \left(\frac{\|f'\|_2^2 [\max f - \min f]}{6} \right)^{\frac{1}{3}}, \quad (13)$$

the MISE of the histogram method decays as $M^{-\frac{2}{3}}$ [22].⁸ Because the computational cost of increasing L and M is negligible, they can be set sufficiently large so that the accuracy of Algorithm 2 mainly depends on the difference between the PDFs of f and f_N^{spline} , denoted by p and \tilde{p} respectively.⁹

To explain why splines are a good choice for density estimation, we first prove

Lemma 3. *Let f be a real, piecewise monotone, continuously differentiable function on $[a, b]$, where $-\infty \leq a < b \leq \infty$, and let μ be an absolutely continuous probability measure on $[a, b]$, i.e., there is $c \in L^1([a, b])$ such that $d\mu(\alpha) = c(\alpha)d\alpha$. Then*

$$p(y) = \sum_{f(\alpha_j)=y} \frac{c(\alpha_j)}{|f'(\alpha_j)|}, \quad (14)$$

where $p(y)$ is the PDF of f .

Proof. See Appendix D. □

Therefore, if $f'(\alpha)$ is bounded away from zero, then p is smooth. As noted, however, the gPC polynomial interpolant $f_N^{\text{gpc}}(\alpha)$ tends to be oscillatory, and so it might add artificial external points where $\frac{d}{d\alpha} f_N^{\text{gpc}}(\alpha) = 0$, see e.g., Fig. 2(c). At every such point where $\frac{d}{d\alpha} f_N^{\text{gpc}}(\alpha) = 0$, the PDF approximation becomes unbounded, and so a large error in the PDF estimation occurs. This is seldom the case with the spline interpolant, which due to its local nature (see Lemma 2) does not produce numerical oscillations throughout its domain Ω . Indeed,

⁷Algorithm 2 can be performed with *any* choice of grid points. For clarity, we present it only with a uniform grid.

⁸In practice, f and f' are often unknown, and so K_f needs to be estimated.

⁹In terms of density estimators, this can be explained by the following argument. Denote by p , p_N , and $\hat{p}_{N,M}$ the density of f , f_N and the density estimator of Algorithm 1 or 2, respectively. Then the approximation error (in any norm) satisfies $\|p - \hat{p}_{N,M}\| \leq \|p - p_N\| + \|p_N - \hat{p}_{N,M}\|$. The second term vanishes as $M \rightarrow \infty$ and L is given by (13), in which case the density estimation error is roughly the bias incurred from approximating f by f_N .

the natural cubic spline $f_N^{\text{spline}}(\alpha)$ has the “minimum curvature” property [37], which implies that it oscillates “very little” about the original function. This notion is made precise by the following result:

Theorem 3. *Let $f \in C^4([\alpha_{\min}, \alpha_{\max}])$ with $|f'(\alpha)| \geq a > 0$, let α be distributed by $c(\alpha)d\alpha$, where $c \in C^1([\alpha_{\min}, \alpha_{\max}])$, and let p and \tilde{p} be the PDFs of $f(\alpha)$ and of its natural, “not-a-knot”, or clamped cubic spline interpolant on a uniform grid of size N , respectively. Then*

$$\|p - \tilde{p}\|_1 \leq KN^{-3}, \quad N > \sqrt[3]{\frac{2C_{\text{spl}}^{(1)} \|f^{(4)}\|_{L^\infty}}{a}} (\alpha_{\max} - \alpha_{\min}), \quad (15)$$

where $C_{\text{spl}}^{(1)}$ is given by Theorem 1 and K depends only on $f(\alpha)$, $c(\alpha)$, and $|\alpha_{\max} - \alpha_{\min}|$.

Proof. See Appendix F. □

Remark. If f is only piecewise C^4 , the N^{-3} convergence is guaranteed when the grid points include the discontinuity points of $f(\alpha)$, since the proof can be repeated in each interval on which the function is C^4 in the same way.

Remark. Although Theorem 3 applies only to functions whose derivatives are bounded away from 0, in practice we observe cubic convergence for non-monotone functions as well (see Sec. 6). Whether Theorem 3 generalizes to non-monotone cases is unclear.

In our numerical simulations, see Figs. 2, 4, 6, and 7, we observe that the cubic convergence is often reached well before N satisfies (15). We also observe that the density approximation error $\|p - \tilde{p}\|_1$ decays at a faster than cubic rate. A possible explanation for this observation is provided by

Lemma 4. *Assume the conditions of Theorem 3, and let J_N be the number of times that $\frac{d}{d\alpha}(f(\alpha) - f_N^{\text{spline}}(\alpha))$ changes its sign on $[\alpha_{\min}, \alpha_{\max}]$. If $J_N = O(N^r)$ for $0 \leq r \leq 1$, then $\|p - \tilde{p}\|_1 \leq KN^{-4+r}$. Specifically, if J_N is uniformly bounded for all $N \in \mathbb{N}$, then $\|p - \tilde{p}\|_1 \leq KN^{-4}$.*

Proof. See Appendix G. □

4.2. Accuracy of moment estimation

Similarly to density estimation, the error of the moment estimation of Algorithm 2 comes from both the numerical integration (step 4) and interpolation (step 2). The trapezoidal rule integration error can be made sufficiently small by increasing the number of samples M at step 4, at a negligible computational cost. Moreover, if $c(\alpha) \equiv 1$, the integration over f_N^{spline} can be done exactly, see footnote 5. Hence, the moment estimation error of Algorithm 2 is determined by the accuracy of the spline interpolation:

Corollary 3. *Let $f \in C^4([\alpha_{\min}, \alpha_{\max}])$, let f_N^{spline} be the natural, “not-a-knot”, or clamped cubic spline interpolant of f , and let α be distributed by $c(\alpha)d\alpha$, where $c(\alpha) \geq 0$, and $\int_{\alpha_{\min}}^{\alpha_{\max}} c(\alpha) d\alpha = 1$. Then*

$$\left| \mathbb{E}_\alpha[f] - \mathbb{E}_\alpha[f_N^{\text{spline}}] \right| \leq C_{\text{spl}}^{(0)} \|f\|_\infty h_{\max}^4,$$

where $C_{\text{spl}}^{(0)}$ and h_{max} are defined in Theorem 1.

Proof. By Theorem 1, $\|f - f_N^{\text{spline}}\|_{\infty} \leq C_{\text{spl}}^{(0)} \|f^{(4)}\|_{\infty} h_{\text{max}}^4$. Hence,

$$\left| \int_{\alpha_{\min}}^{\alpha_{\max}} (f(\alpha) - f_N^{\text{spline}}(\alpha)) c(\alpha) d\alpha \right| \leq$$

$$\|f - f_N^{\text{spline}}\|_{\infty} \int_{\alpha_{\min}}^{\alpha_{\max}} c(\alpha) d\alpha \leq \|f - f_N^{\text{spline}}\|_{\infty} \cdot 1 \leq C_{\text{spl}}^{(0)} \|f^{(4)}\|_{\infty} h_{\text{max}}^4.$$

□

Typically, $C_{\text{spl}}^{(0)} < 1$. For example, for the natural and “not-a-knot” cubic spline, $C_{\text{spl}}^{(0)}$ is equal to $\frac{5}{384}$ and $\frac{1}{25}$, respectively [30, 34]. On a uniform grid, $h_j = \frac{\alpha_{\max} - \alpha_{\min}}{N-1}$ for $1 < j \leq N$, and so $\mathbb{E}_{\alpha}[f] - \mathbb{E}_{\alpha}[f_N^{\text{spline}}] = O(N^{-4})$.

As $N \rightarrow \infty$, the *polynomial* convergence rate of the spline approximation (Corollary 3) is outperformed by gPC’s *spectral* convergence rate (Corollary 1). Quite often, however, the spline approximation is more accurate for *moderate* N values. To see that, note that by (6), (9), and (10), $\mathbb{E}_{\alpha}[f_N^{\text{gpc}}] = \sum_{j=1}^N f(\alpha_j) w_j$, which is the Gauss quadrature rule. Hence, if $f \in C^{2N}$, then

$$\mathbb{E}_{\alpha}[f] - \mathbb{E}_{\alpha}[f_N^{\text{gpc}}] = \frac{f^{(2N)}(\xi)}{k_N^2 (2N)!}, \quad \xi \in (\alpha_{\min}, \alpha_{\max}),$$

where k_N is the leading coefficient of $p_N(\alpha)$ [28]. If for small N , $\|f^{(2N)}\|_{\infty}$ increases faster than $k_N^2 (2N)!$, the error initially *increases* with N . In these cases, the exponential convergence is only achieved at large N .¹⁰ Even when gPC does converge exponentially, i.e., $|\mathbb{E}_{\alpha}[f] - \mathbb{E}_{\alpha}[f_N^{\text{gpc}}]| \leq K e^{-\gamma N}$, if γ is small, the error of the spline approximation may be smaller for moderate values of N , see e.g., Fig. 1(c).

To conclude, unlike for gPC, the accuracy of spline-based moment approximation is *guaranteed* also with few samples.

5. Toy example

In this section, we approximate the function

$$f(\alpha) = \tanh(9\alpha) + \frac{\alpha}{2}, \quad \alpha \in [-1, 1], \quad (16)$$

which is an example of a smooth function with a narrow high-derivative region.¹¹

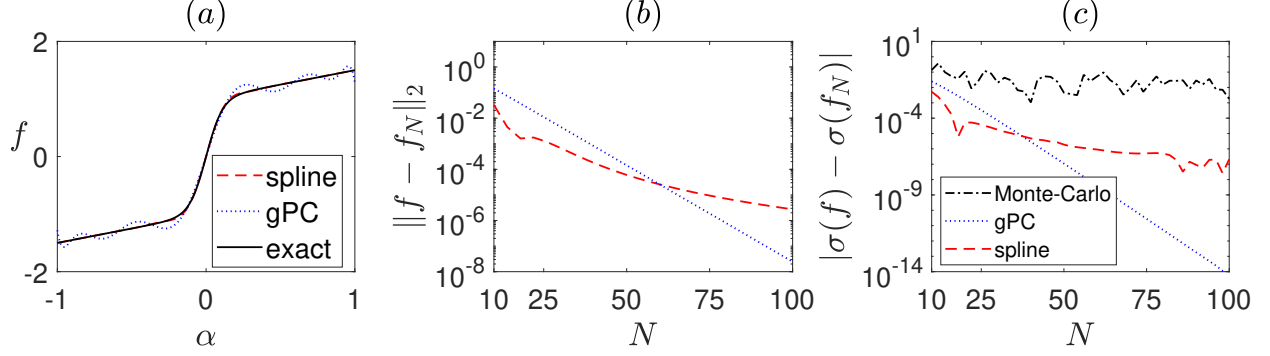


Figure 1: (a) $f(\alpha)$ (solid), see (16), and its spline interpolant (dashes) are nearly indistinguishable, whereas the gPC interpolant (dots) oscillates “around” f . Both interpolants use $N = 12$ grid points. (b) L^2 error of both interpolants as a function of the number of samples. (c) Error of the standard deviation when it is approximated using Monte-Carlo method (dash-dot), the gPC-based method (dots) and the spline-based method (dashes).

5.1. Interpolation

With $N = 12$ samples, the spline interpolant f_N^{spline} of (16) is nearly indistinguishable from f , whereas the gPC interpolant f_n^{gpc} slightly oscillates “around” f , see Fig. 1(a). Although f_N^{gpc} converges exponentially to f in L^2 , see Fig. 1(b), its L^2 approximation error $\|f - f_N\|_2 = (\int_{-1}^1 |f(\alpha) - f_N(\alpha)|^2 d\alpha)^{\frac{1}{2}}$ with few samples ($10 \leq N \leq 40$) is larger than that of the spline interpolant by more than an order of magnitude. With sufficiently many samples ($N > 70$), however, the gPC approximation exponential convergence outperforms the spline’s polynomial convergence rate. This example shows that with few samples, the occurrence of a “jump” in f hurts the accuracy of the gPC interpolant. Spline interpolation, on the other hand, is less sensitive to the “jump”, because it “confines” the approximation error induced by the jump to the jump interval (roughly $\alpha \in (-0.1, 0.1)$), see Lemma 2.

5.2. Moment approximation

The interpolation accuracy is relevant to moment approximation, because a small L^2 error implies a small moment-approximation error (Lemma 1). For example, Fig. 1(c) shows the standard deviation error $|\sigma(f) - \sigma(f_N)|$, see (16), when α is uniformly distributed in $[-1, 1]$. As expected, the spline-based method (Algorithm 2) is more accurate than the gPC-based method (Algorithm 1) with few samples, but the gPC is more accurate with sufficiently many samples. A purely statistical approach such as Monte-Carlo converges poorly compared to both the spline and gPC approach, with about 10% error with $N \leq 100$ sample points.

5.3. Density estimation

Consider the PDF induced by $f(\alpha)$, see (16), when α is uniformly distributed in $[-1, 1]$. The PDF computed by the gPC-based Algorithm 1 with $N = 18$ sample points deviates considerably from the exact PDF, see Fig. 2(a), whereas the PDF computed by the spline-based

¹⁰For example, if the numerator grows as K^{2N} , the error only decays for $N > K$.

¹¹The $\frac{\alpha}{2}$ term was added so that $\frac{df}{d\alpha}$ is bounded away from zero, in order to prevent singularities in the PDF, see Sec. 5.3

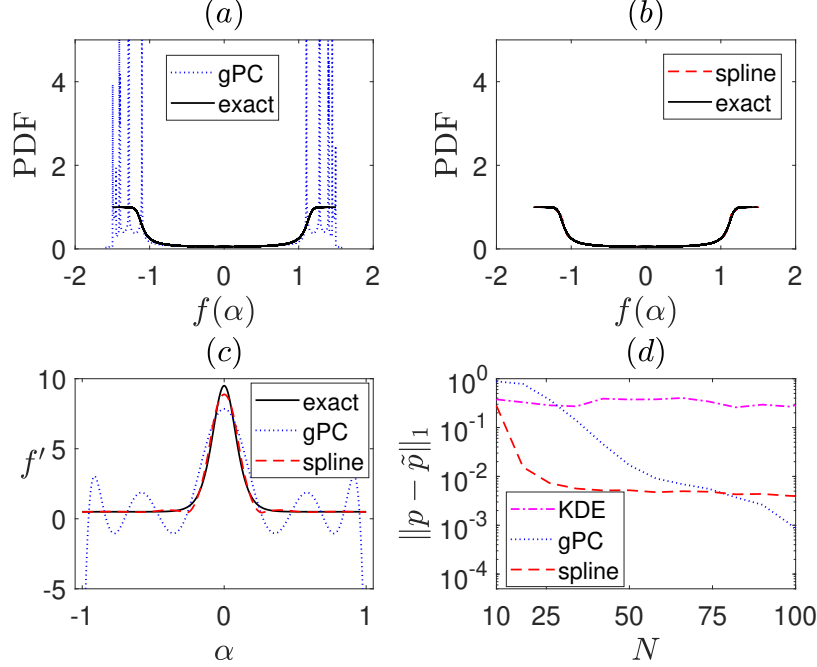


Figure 2: The PDF of $f(\alpha)$, see (16), where α is uniformly distributed in $[-1, 1]$. (a) exact PDF (solid) and its approximation by the gPC-based Algorithm 1 (dots) with $N = 18$ sample points. (b) Same, with the spline-based Algorithm 2 (dashes). The two lines are nearly indistinguishable. (c) Derivatives of f (solid), f_N^{spline} (dashes) and f_N^{gpc} (dots). (d) L^1 error of the PDF approximations as a function of the number of sample points, for the KDE (dash-dot), gPC-based approximation (dots), the spline-based approximation (dashes), and its power-law fit $103.2N^{-3.29}$ (solid).

Algorithm 2 with $N = 18$ sample points is nearly indistinguishable from the exact PDF, see Fig. 2(b).¹² This is consistent with our discussion in Sec. 4. Indeed, the derivative of the spline interpolant $\frac{d}{d\alpha} f_N^{\text{spline}}$ approximates $f'(\alpha)$ with cubic accuracy, whereas the derivative of the gPC interpolant $\frac{d}{d\alpha} f_N^{\text{gpc}}$ has many artificial extremal points where $\frac{d}{d\alpha} f_N^{\text{gpc}}(\alpha) = 0$, but $\frac{d}{d\alpha} f(\alpha) \neq 0$, see Fig. 2(c).

The L^1 distance $\|p - \tilde{p}\|_1$ between the exact PDF p and its approximation \tilde{p} is presented in Fig. 2(d). For $10 \leq N \leq 100$ the spline-based approximation is more accurate than the gPC-based one by nearly two orders of magnitude. This is in contrast to moment estimation, see Fig. 1(c), in which the gPC approximation becomes more accurate for $N \geq 40$. Furthermore, we observe numerically that the spline-based method converges even faster than the N^{-3} rate predicted by Theorem 3. The KDE approximation has roughly 10% error for $N \leq 100$.¹³ Other frequently-used distances between distributions, such as the Hellinger

¹²The MATLAB code that generates this PDF approximation is given in Appendix E.

¹³The poor accuracy of the KDE method is due to the fact that the KDE does not use the “functional information” $\{f_j = f(\alpha_j)\}_{j=1}^N$, but only the set $\{f_j\}_{i=1}^N$.

distance $\frac{1}{\sqrt{2}} \|\sqrt{p} - \sqrt{\tilde{p}}\|_2$ [38] and the Kullback-Leibler (KL) Divergence¹⁴ [39]

$$\int_{-\infty}^{\infty} p(y) \log \left(\frac{p(y)}{\tilde{p}(y)} \right) dy, \quad (17)$$

produce similar results (data not shown).

5.4. Density estimation of non-smooth functions

Let

$$g(\alpha) = f(\alpha) \bmod (0.7), \quad (18)$$

where f is given by (16).¹⁵ Because (18) is non-smooth, with few samples neither the spline, nor the gPC interpolant are even remotely close to $g(\alpha)$, see Fig. 3. Therefore, to approximate the PDF associated with $g(\alpha)$, we first use Algorithms 1 and 2 to approximate $f(\alpha) \approx f_N(\alpha)$. Since f is smooth, both approximations are reasonable with few samples, see Fig. 1. Next, we approximate $g(\alpha_m) \approx f_N(\alpha_m) \bmod (0.7)$, and compute the PDF of g using the histogram method on a high-resolution sampling grid ($M = 2 \cdot 10^6$). We again stress that evaluating f_N is computationally cheap, and therefore can be easily done with such a large sample. As in the smooth case, see Fig. 2, the PDF approximated by the gPC-based Algorithm 1 with $N = 18$ sample points has large deviations and converges poorly, see Fig. 4(a), whereas the PDF approximated by the spline-based Algorithm 2 with $N = 18$ sample points is nearly identical to the exact PDF, see Fig. 4(b). Indeed the L^1 error of spline-based PDF is smaller than that of the gPC-based PDF by at least an order of magnitude, for $20 < N < 50$, see Fig. 4(c). Although Theorem 3 applies only to C^4 functions, we observe numerically that the convergence rate of the spline-based PDF is faster than N^{-3} . The KDE approximation for the PDF of $g(\alpha)$ is poorer than that of the spline-based and gPC-based approximations.

6. Application 1 - nonlinear Schrödinger equation

The one-dimensional coupled nonlinear Schrödinger equation (CNLS)

$$i \frac{\partial A_{\pm}(t, x)}{\partial t} + \frac{\partial^2 A_{\pm}}{\partial x^2} + \frac{2}{3} \frac{|A_{\pm}|^2 + 2|A_{\mp}|^2}{1 + \epsilon (|A_{\pm}|^2 + |A_{\mp}|^2)} A_{\pm} = 0, \quad (19)$$

where $0 < \epsilon \ll 1$, $t \geq 0$, and $x \in \mathbb{R}$, describes the propagation of elliptically polarized, ultra-short pulses in optical fibers [40], of elliptically polarized continuous-wave (CW) beams in a bulk medium [41, 42], Stokes and anti-Stokes radiation in Raman amplifiers [43], and rogue

¹⁴Intuitively, the d_{KL} measures the entropy added, or conversely, the information lost, in approximating p by \tilde{p} .

¹⁵This example is motivated by our study of the NLS [8], where the cumulative phase $\varphi(t; \alpha) = \arg[\psi(t, 0; \alpha)]$ is smooth, but the quantity of interest, the angle $\varphi \bmod (2\pi)$, is discontinuous. See Sec. 6. for another optics application which motivates this example.

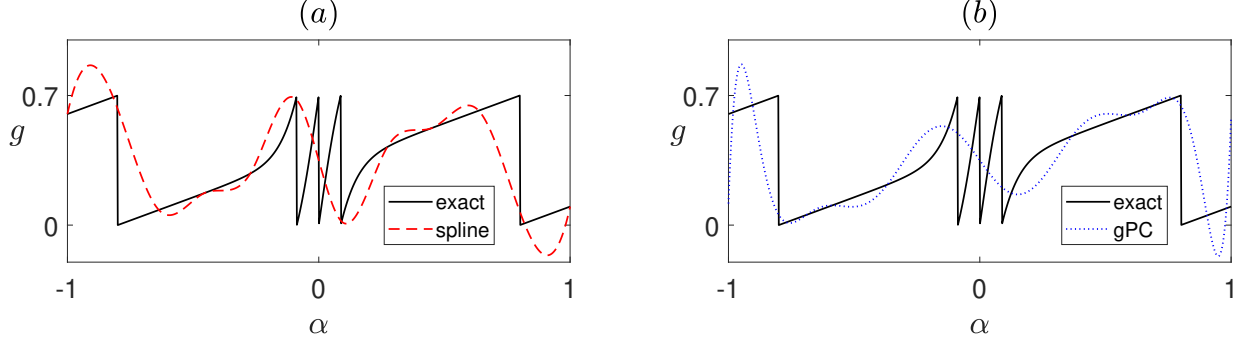


Figure 3: The discontinuous function $g(\alpha)$, see (18) (solid), and its spline interpolation with $N = 12$ sample points (dashes). (b) Same with the gPC interpolant (dots).

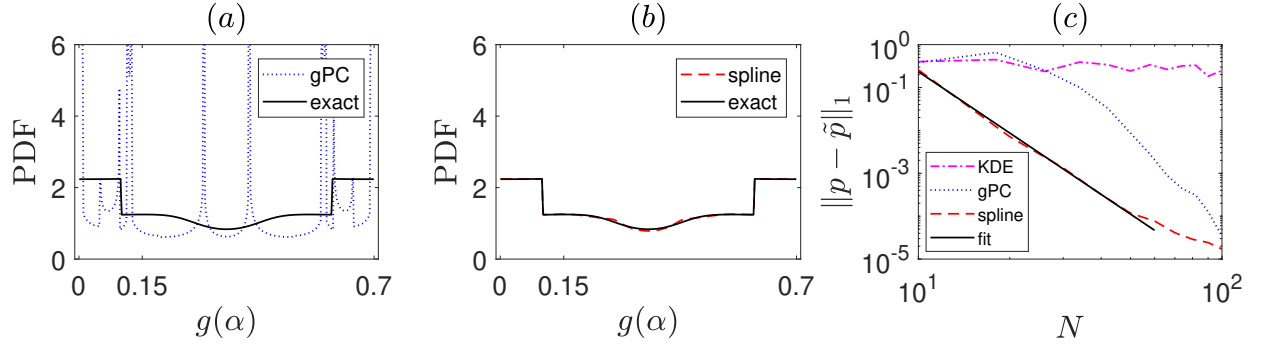


Figure 4: Same as Fig. 2 for the discontinuous function $g(\alpha)$, see (18). The solid line in subplot (c) is the power-law fit $1.33 \cdot 10^4 N^{-4.75}$ of the spline-based approximate PDF.

water-waves formation at the interaction of crossing seas [44]. We consider (19) with an elliptically-polarized Gaussian input pulse with a random amplitude [42, 41]

$$\begin{pmatrix} A_+ \\ A_- \end{pmatrix} = (1 + 0.1\alpha) \begin{pmatrix} 8 \\ 4 \end{pmatrix} e^{-x^2}, \quad (20)$$

where A_+ and A_- are the clockwise and counter-clockwise circularly-polarized components, respectively. The *on-axis ellipse rotation angle* is defined as

$$\theta(t; \alpha) := (\varphi_+(t; \alpha) - \varphi_-(t; \alpha)) \bmod (2\pi), \quad (21)$$

where $\varphi_{\pm}(t; \alpha) := \arg[A_{\pm}(t, 0; \alpha)]$ are the on-axis phases of the components. The distribution of $\theta(t; \alpha)$ indicates to what extent the ellipse rotation angle is “deterministic”.¹⁶

Interpolation. For a given sample grid $\{\alpha_j\}_{j=1}^N$, we compute $\theta(t; \alpha_j)$ for each $1 \leq j \leq N$ by solving (19)–(20) and using (21). Fig. 5(a) shows the spline and gPC interpolants of

¹⁶We solve the CNLS using a fourth-order, compact finite-difference scheme for the spatial discretization, and a predictor-corrector Crank-Nicolson scheme for the temporal integration of the semi-discrete problem [45].

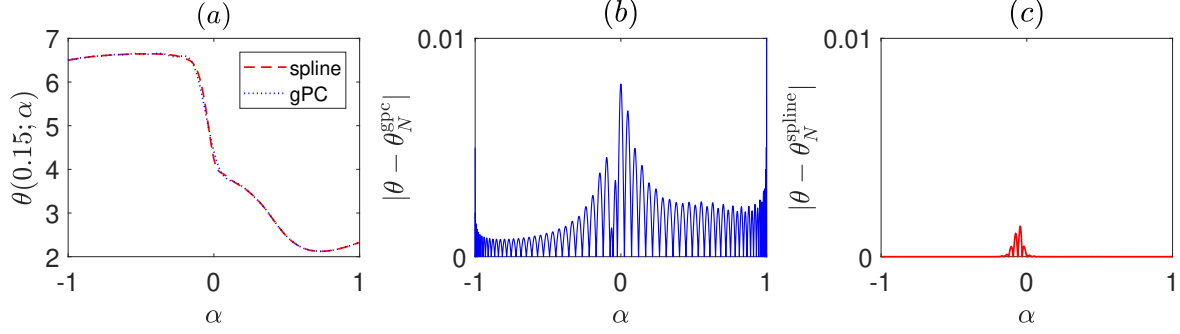


Figure 5: The polarization angle $\theta(t = 0.15; \alpha)$ for solutions of the CNLS (20) with $\epsilon = 10^{-5}$, and an elliptically polarized Gaussian initial condition (20). (a) Spline interpolation (dashes) and gPC interpolation (dots), with $N = 64$ sample points. The two lines are nearly indistinguishable. (b) Pointwise error of the gPC interpolant. (c) Same for the spline interpolant.

$\theta(t = 0.15; \alpha)$ with $N = 64$ points.¹⁷ While these interpolants seem nearly identical, the spline interpolant is more accurate than the gPC interpolant by more than an order of magnitude (cf. Figs. 5(b) and 5(c)). Indeed, the L^2 error of the gPC interpolant (0.17%) is an order of magnitude larger than that of the spline interpolant (0.017%).

Density estimation. The spline-based approximated PDF with $N = 64$ sample points is indistinguishable from the exact PDF, see Fig. 6(a). In contrast, the gPC-based approximation with $N = 64$ differs substantially from the exact PDF, see Fig. 6(b). Indeed, the KL divergence of the gPC-based approximation, see (17), is *about 16,000 times larger* than that of the spline-based approximation, and the L^1 error is 200 times larger (46% vs. 0.2%). With $N = 32$, the spline-based is *32 times more accurate* than the gpc-approximated PDF, in term of KL divergence, and 11 time more accurate in terms of the L^1 error (41% vs. 4.5%). The L^1 error of the spline-based PDF decays as $N^{-3.76}$, see Fig. 6(c), in accordance with Theorem 3. Since the PDF of $\theta(0.15; \alpha)$ has discontinuities and high derivatives, spline smoothing techniques and KDE methods with smooth kernels were not considered in this case.

Moment approximation. The mean and standard deviation of circular quantities can be defined as [46]¹⁸

$$\mathbb{E}_\alpha^{\text{circ}}[\theta(t; \alpha)] = \int_{-1}^1 e^{i\theta(t; \alpha)} d\alpha, \quad \sigma^{\text{circ}}(\theta) = \sqrt{-2 \ln |\mathbb{E}_\alpha^{\text{circ}}[\theta(t; \alpha)]|}. \quad (22)$$

¹⁷Because we have no explicit solution for $\theta(t; \alpha)$, the errors in this section are measured by comparison with $\theta_{513}^{\text{spline}}(0.15, \alpha)$ with $N = 513$ sample points. We verified that $\|\theta_{513}^{\text{spline}}(0.15, \alpha) - \theta_{513}^{\text{gpc}}(0.15, \alpha)\|_2 \approx 5 \cdot 10^{-5}$, which is an order of magnitude smaller than the approximation errors noted in the text.

¹⁸To motivate why a different definition for circular moments is needed, consider $y \sim U(-\pi, \pi)$ and $z \sim U(0, 2\pi)$. If we consider y and z as *angles*, or points on the circle, they are identical. Using the conventional mean definition, however, yields $\mathbb{E}[y] = 0$, but $\mathbb{E}[z] = \pi$.

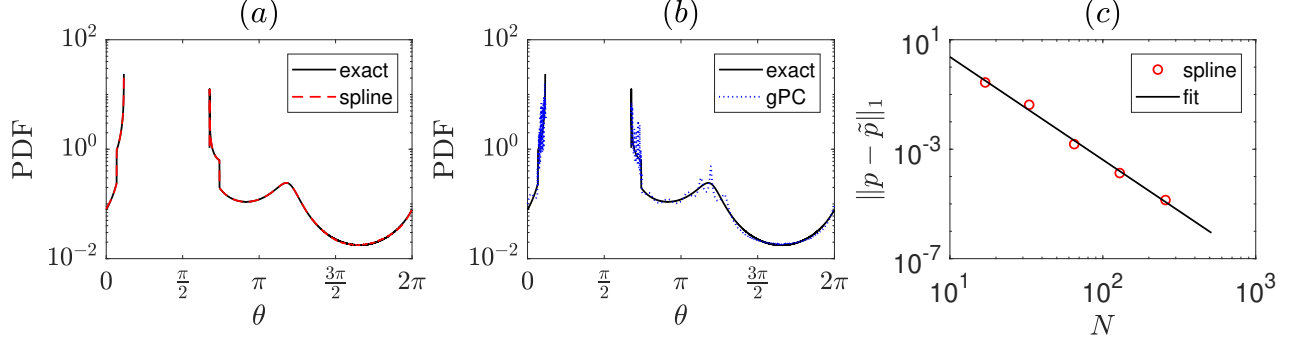


Figure 6: Same settings as in Fig. 5. The PDF of $\theta(0.15, \alpha)$, where $\alpha \sim U(-1, 1)$. (a) Exact PDF (solid), and spline-based approximation using $N = 64$ sample points (dashes). The two lines are indistinguishable. (b) Same with the gPC-based PDF approximation (dots). (c) L^1 error of the spline-based PDF as a function of N (circles) and the power-law fit $1.35 \cdot 10^4 N^{-3.76}$ (solid).

The advantage of splines over gPC with few samples for moments approximation can be seen in Table 1. The approximation of $\mathbb{E}_\alpha^{\text{circ}}[\theta(0.15; \alpha)]$ using the spline approximation with $N = 32$ is 4 times more accurate than that of the gPC; with $N = 64$ it is 14 times more accurate. The approximation of the standard deviation using the spline-based method with $N = 32$ is 12 times more accurate than the gPC; with $N = 64$ it is 33 times more accurate than the gPC-based approximation.

	N	gPC error	spline error	$\frac{\text{gPC error}}{\text{spline error}}$
$\mathbb{E}_\alpha^{\text{circ}}[\theta(0.15; \alpha)]$	32	2.2%	0.54%	4
$\mathbb{E}_\alpha^{\text{circ}}[\theta(0.15; \alpha)]$	64	0.089%	0.006%	14
$\sigma^{\text{circ}}(\theta(0.15; \alpha))$	32	0.64%	0.054%	12
$\sigma^{\text{circ}}(\theta(0.15; \alpha))$	64	0.031%	0.0009%	33

Table 1: Approximation error of the circular mean and standard deviation, see (22), of $\theta(0.15, \alpha)$, see (21), with gPC- and spline-based approximations, using N sample points.

7. Application 2 - inviscid Burgers equation

The inviscid Burgers equation

$$u_t(t, x) + \frac{1}{2}(u^2)_x = \frac{1}{2}(\sin^2(x))_x, \quad x \in [0, \pi], \quad t \geq 0, \quad (23)$$

with the initial and boundary conditions $u(0, x) = u_0(x)$ and $u(t, 0) = u(t, \pi) = 0$ models isentropic gas flow in a dual-throat nozzle. Solutions of this equation can develop a static shock wave at a lateral location $x = X_s$ [47]. Following [4], we consider the case in which α is a random variable with a known distribution, $u_0(x) = u_0(x; \alpha)$ is random, and we wish to compute the PDF of X_s using Algorithms 1 and 2. In general, to do that requires, for each $1 \leq j \leq N$, to compute $X_s(\alpha_j)$ by solving (23) with α_j . For the special initial condition

$$u_0(x) = \alpha \sin(x), \quad (24a)$$

however, the shock location is explicitly given by [4]

$$\alpha = -\cos(X_s) . \quad (24b)$$

This explicit expression allows us to sample $X_s(\alpha)$ without solving (23).

Consider the case where

$$\alpha = \begin{cases} \frac{-1+\sqrt{1+4\nu^2}}{2\nu} & \text{if } \nu \neq 0, \\ 0 & \text{if } \nu = 0, \end{cases} \quad (25)$$

and $\nu \sim \mathcal{N}(0, \sigma)$, i.e., it is normally distributed with a zero mean. Because α is not distributed by a classical, standard measure, there is no obvious choice of quadrature points to sample by, nor is there a “natural” orthogonal polynomials basis to expand the solution by. Therefore, the gPC approach cannot be straightforwardly applied.¹⁹ We can, however, apply the gPC approach to this problem by denoting $X_s(\nu) = X_s(\alpha(\nu))$, and approximating $X_s(\nu)$ using the Hermite polynomials (which are orthogonal with respect to the normal distribution).²⁰ The gPC-based approximated PDF with $N = 7$ sample points differs considerably from the exact PDF, see Fig. 7(a). In contrast, the spline-based approximated PDF can be directly applied to $X_s(\alpha)$, and it is nearly indistinguishable from the exact PDF already with $N = 7$ sample points, see Fig. 7(b). In general, the spline-based PDF approximation is more accurate than the gPC-based approximation by more than one order of magnitude for $5 < N < 50$, see Fig. 7(c). The L^1 error of the spline-based PDF is observed numerically to decay as $N^{-3.11}$, in accordance with Theorem 3.

We repeated these simulations for the case with $\alpha \sim B(r, s)$, where $B(r, s)$ is the Beta distribution on $[-1, 1]$.²¹ The spline based approximations are nearly identical to the exact PDF, whereas the gPC method were less accurate by an order of magnitude with few samples (results not shown).

8. Discussion

In this paper, we introduced a spline-based method for density and moment estimation. The advantages of this method are:

1. It approximates the density at a guaranteed cubic convergence rate.
2. It provides reasonable approximations for the density and moments using small sample sizes.
3. Its accuracy is relatively unimpaired by the presence of large derivatives.
4. It is non-intrusive, i.e., it is based solely on solving the underlying deterministic model.

¹⁹Nevertheless, even for non-standard distributions, the expansion of α by a classical orthogonal polynomials basis can still converge spectrally, under certain conditions [48].

²⁰Indeed, in [4] the authors use the gPC-Galerkin method with the Hermite polynomials [49, 19].

²¹The PDF of the Beta distribution on $[0, 1]$ is $p(\alpha) = \frac{(\alpha^{r-1}(1-\alpha)^{s-1}\Gamma(r+s))}{\Gamma(r)\Gamma(s)}$.

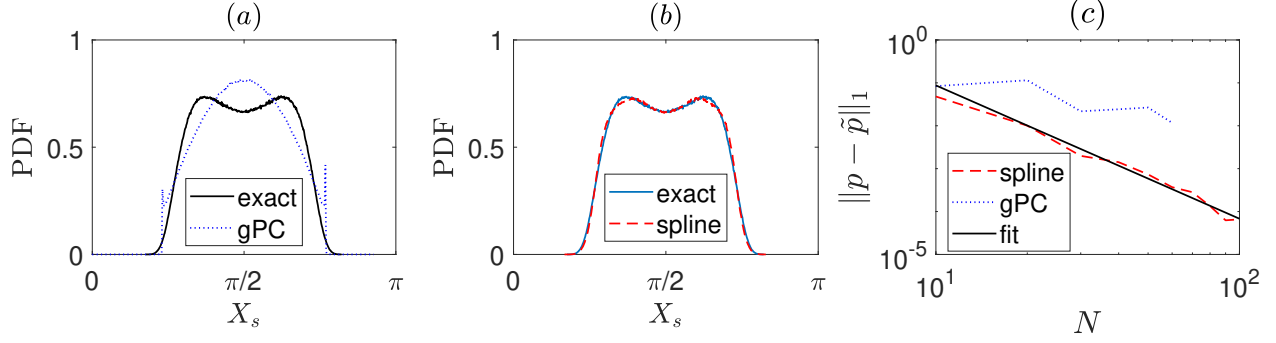


Figure 7: PDF of $X_s(\alpha)$, where $\alpha(\nu)$ is given by (25), and $\nu \sim \mathcal{N}(0, 0.6)$. (a) Exact PDF (solid) and gPC-based approximation (dots) with $N = 7$ sample points. (b) Same with the spline-based approximation (dashes). (c) L^1 error of the PDF approximations as a function of the number of sample points, and the power-law fit $112N^{-3.11}$ (solid).

5. It is easy to implement.
6. It is applicable with any choice of sample points.
7. It can be applied to non-smooth quantities of interest.

The choice of the histogram method to estimate the density was motivated by four factors:

1. Implementing the histogram method is straightforward, and can be done with a few lines of code (see Appendix E).
2. The accuracy of the histogram method can be improved and controlled by varying the number of samples M , with a negligible computational cost.
3. The histogram method can be used even when the quantity of interest f is not smooth.
4. The histogram method can be used for a multi-dimensional random parameter α .

In principle, we could have used the explicit relation (14) to compute the PDF. Because this approach does not have the above advantages, however, the histogram method was chosen.

This paper focuses on a one-dimensional noise parameter (i.e., $\alpha \in \Omega \subseteq \mathbb{R}$). Since the case of multi-dimensional noise (i.e., $\alpha \in \Omega \subseteq \mathbb{R}^d$) is frequently found in applications, it is natural to extend our approach to higher dimensions using multivariate spline approximations [50]. A systematic study of spline-based methods for multi-dimensional moments and PDF estimation is a goal of our future study. Furthermore, in very high-dimensional noises, for a given resolution at each dimension, N grows exponentially with the dimension d (the “curse of dimensionality”). One popular approach for this problem is the use of sparse sample grids [15, 10]. Whether spline-based methods can be extended to such grids is also left to future research.

When $f \in C^{m+1}$, it is tempting to use splines of order $m > 3$ for density estimation, in order to attain faster than cubic convergence rate. If one generalizes Algorithm 2 to splines of order m then, similarly to Theorem 3, a convergence of order N^{-m} is guaranteed. Even if f is analytic, however, it is not advisable to take a large m , for two reasons. First, for

$s(\alpha)$ to be monotone (and so, by Lemma 3 for the PDF to be continuous), N should scale as $\sqrt[m]{\|f^{(m+1)}\|_\infty}$, see (F.1). Therefore, for a large m , high-order convergence might only be attained for very large sample sizes. Second, the density approximation error depends linearly on $\|f^{(m+1)}\|_\infty$, see Appendix F, and so it might “blow-up” exponentially with m . To conclude, although we do not know whether the optimal spline order is $m = 3$, an arbitrarily high-order spline should not be used.

In this paper we showed that spline-based density estimation is better than gPC-based density estimation, because it does not produce numerous artificial extremal points (see Lemma 3). An interpolating cubic spline, however, might still produce artificial extremal points, though not as much as the gPC polynomial. To absolutely prevent artificial extremal points from being produced, it may be better to use spline interpolants [51] and quasi-interpolants [52] which are *monotonicity-preserving* (i.e., splines which are monotone wherever the sampled data is monotone). We leave it to future research to check whether monotonicity-preserving interpolants provide more accurate PDF approximations than a standard interpolating cubic spline.

9. Acknowledgments

This research of A. Ditkowski was supported by the United States - Israel Binational Science Foundation (BSF) [grant Number 2016197]. The research of G. Fibich and A. Sagiv was partially supported by the Israel Science Foundation (ISF) [grant number 177/13]. The authors want to thank Y. Harness, B. Brill, R. Kats, F. Abramovich, and D. Levin for useful comments and conversations.

References

- [1] H.N. Najm. Uncertainty quantification and polynomial chaos techniques in computational fluid dynamics. *Ann. Rev. Fluid Mech.*, 41:35–52, 2009.
- [2] O.P. Le Maître, L. Mathelin, O.M. Knio, and M.Y. Hussaini. Asynchronous time integration for polynomial chaos expansion of uncertain periodic dynamics. *Discrete Contin. Dyn. Syst.*, 28:199–226, 2010.
- [3] O. Le Maître and O.M. Knio. *Spectral Methods for Uncertainty Quantification: With Applications to Computational Fluid Dynamics*. Springer, New-York, 2010.
- [4] Q.Y. Chen, D. Gottlieb, and J.S. Hesthaven. Uncertainty analysis for the steady-state flows in a dual throat nozzle. *J. Comp. Phys.*, 204:378–398, 2005.
- [5] B. Ganapathysubramanian and N. Zabaras. Sparse grid collocation schemes for stochastic natural convection problems. *J. Comp. Phys.*, 225:652–685, 2007.
- [6] B. Sudret and A. Der Kiureghian. *Stochastic Finite Element Methods and Reliability: a State-of-the-Art Report*. Department of Civil and Environmental Engineering, University of California Berkeley, Berkeley, CA, 2000.
- [7] G. Porta, L. Tamellini, V. Lever, and M. Riva. Inverse modeling of geochemical and mechanical compaction in sedimentary basins through polynomial chaos expansion. *Water Resources Research*, 50:9414–9431, 2014.
- [8] A. Sagiv, A. Ditzkowski, and G. Fibich. Loss of phase and universality of stochastic interactions between laser beams. *Opt. Exp.*, 25:24387–24399, 2017.
- [9] S. Ullmann. *POD-Galerkin Modeling for Incompressible Flows with Stochastic Boundary Conditions*. M.Sc. dissertation, Technical University of Darmstadt, 2014.
- [10] R. Ghanem, D. Higdon, and H. Owhadi. *Handbook of Uncertainty Quantification*. Springer, New York, 2017.
- [11] A. Der Kiureghian and J.B. Ke. The stochastic finite element method in structural reliability. *Prob. Eng. Mech.*, 3:83–91, 1988.
- [12] R.G. Ghanem and P.D. Spanos. *Stochastic Finite Elements: a Spectral Approach*. Springer-Verlag, New-York, 1991.
- [13] B.J. Debuschere, H.N. Najm, P.P. Pébay, O.M. Knio, R.G. Ghanem, and O. Le Maître. Numerical challenges in the use of polynomial chaos representations for stochastic processes. *SIAM J. Sci. Comp.*, 26:698–719, 2004.
- [14] G. Stefanou. The stochastic finite element method: past, present and future. *Comp. Meth. Appl. Mech. Eng.*, 198:1031–1051, 2009.
- [15] D. Xiu. *Numerical Methods for Stochastic Computations: a Spectral Method Approach*. Princeton University Press, Princeton, NJ, 2010.

- [16] A. O'Hagan. Polynomial chaos: A tutorial and critique from a statistician's perspective. *SIAM/ASA J. Uncertainty Quantification*, 20:1–20, 2013.
- [17] X. Wan and G.E. Karniadakis. An adaptive multi-element generalized polynomial chaos method for stochastic differential equations. *J. Comput. Phys.*, 209:617–642, 2005.
- [18] O.P. Le Maître, O.M. Knio, H.N. Najm, and R.G. Ghanem. Uncertainty propagation using wiener–haar expansions. *J. Comp. Phys.*, 197:28–57, 2004.
- [19] D. Xiu and G.E. Karniadakis. The Wiener–Askey polynomial chaos for stochastic differential equations. *SIAM J. Sci. Comput.*, 24:619–644, 2002.
- [20] D. Xiu and J.S. Hesthaven. High-order collocation methods for differential equations with random inputs. *SIAM J. Sci. Comput.*, 27:1118–1139, 2005.
- [21] A.J. Izenman. Review papers: recent developments in nonparametric density estimation. *J. Am. Stat. Assoc.*, 86:205–224, 1991.
- [22] L. Wasserman. *All of Statistics: A Concise Course in Statistical Inference*. Springer Science & Business Media, New York, 2004.
- [23] A. B. Tsybakov. *Introduction to Nonparametric Estimation*. Springer, New York, 2009.
- [24] R.J. Field and R.M. Noyes. Oscillations in chemical systems. IV. Limit cycle behavior in a model of a real chemical reaction. *J. Chem. Phys.*, 60:1877–1884, 1974.
- [25] G. Szego. *Orthogonal Polynomials*, Colloquium Publications, Vol. 23. American Mathematical Soc., New York, 1939.
- [26] H. Wang and S. Xiang. On the convergence rates of Legendre approximation. *Math. Comp.*, 81:861–877, 2012.
- [27] L.N. Trefethen. *Approximation Theory and Approximation Practice*. SIAM, Philadelphia, PA, 2013.
- [28] P.J. Davis and P. Rabinowitz. *Numerical Integration*. Blaisdell, Waltham, Mass., 1967.
- [29] J. S. Hesthaven, S. Gottlieb, and D. Gottlieb. *Spectral Methods for Time-Dependent Problem* Cambridge, UK, 2007.
- [30] C. A. Hall and W. W. Meyer. Optimal error bounds for cubic spline interpolation. *J. Approx. Theory*, 16:105–122, 1976.
- [31] R. K. Beatson. On the convergence of some cubic spline interpolation schemes. *SIAM J. Numer. Anal.* 23:903–912, 1986.
- [32] G. Birkhoff and C. De Boor. Error bounds for spline interpolation. *J. Math. Mech.*, 13:827–836, 1964.
- [33] C. De Boor. On cubic spline functions that vanish on all knots. *Adv. Math.*, 20:1–17, 1976.

- [34] R. K. Beatson and E. Chacko. Which cubic spline should one use? *SIAM J. Sci. Stat. Comput.* 13:1009–1024, 1992.
- [35] G. Wahba. *Spline Models for Observational Data*. SIAM, 1990.
- [36] R.L. Eubank. *Nonparametric Regression and Spline Smoothing*. Mercel Dekker, New York, 1999.
- [37] P.M. Prenter. *Splines and Variational Methods*. Courier Corporation, New-York, 2008.
- [38] L. Le Cam and G. L. Yang. *Asymptotics in Statistics: Some Basic Concepts*. Springer Science & Business Media, New York, 2012.
- [39] S. Kullback and R.A. Leibler. On information and sufficiency. *Ann. Math. Stat.*, 22:79–86, 1951.
- [40] G.P. Agrawal. *Nonlinear Fiber Optics*. 5th edition, Academic Press, 2012.
- [41] G. Patwardhan, X. Gao, A. Dutt, J. Ginsberg, and A.L. Gaeta. Loss of polarization in collapsing beams of elliptical polarization. In *Conference on Lasers and Electro-Optics (CLEO)*, pages 1–2. OSA, 2017.
- [42] A.H. Sheinfux, E. Schleifer, J. Papeer, G. Fibich, B. Ilan, and A. Zigler. Measuring the stability of polarization orientation in high intensity laser filaments in air. *Applied Physics Letters*, 101(20):201105, 2012.
- [43] S. Randoux, N. Dalloz, and P. Suret. Intracavity changes in the field statistics of Raman fiber lasers. *Opt. Lett.*, 36:790–792, 2011.
- [44] M.J. Ablowitz and T.P. Horikis. Interacting nonlinear wave envelopes and rogue wave formation in deep water. *Phys. Fluids*, 27:012107, 2015.
- [45] G. Fibich. *The Nonlinear Schrödinger Equation*. Springer, New York, 2015.
- [46] K.V. Mardia and P.E. Jupp. *Directional Statistics*. John Wiley & Sons, Chichester, UK, 2009.
- [47] M.D. Salas, S. Abarbanel, and D. Gottlieb. Multiple steady states for characteristic initial value problems. *Appl. Numer. Math.*, 2:193–210, 1986.
- [48] A. Ditkowski and R. Kats. On spectral approximations with nonstandard weight functions and their implementations to generalized chaos expansions. *arXiv preprint arXiv:1611.00242*, 2016.
- [49] R.G. Ghanem and P. Spanos. *Stochastic Finite Elements: A Spectral Approach*. Springer-Verlag, New-York, 1991.
- [50] C.K. Chui. *Multivariate Splines*. SIAM, Philadelphia, PA, 1988.
- [51] F.N. Fritsch and R.E. Carlson. Monotone piecewise cubic interpolation. *SIAM J. Numer. Anal.*, 17:238–246, 1980.

- [52] C. De Boor. *A Practical Guide to Splines*. Springer-Verlag, New York, 1978.
- [53] S. Demko, W. F. Moss, and P. W. Smith. Decay rates for inverse of band matrices *Math. Comp.* 43:491–499, 1984.
- [54] G. H. Golub and C. F. Van Loan. *Matrix Computations*. JHU, Baltimore, MD, 2012.
- [55] C. R. Johnson. Positive definite matrices. *Amer. Math. Month.* 77:259–264.

Appendix A. Proof of Lemma 1

For all $f, g \in L^2$,

$$\left| \mathbb{E}_\alpha[f] - \mathbb{E}_\alpha[g] \right| \leq \int_\Omega |f(\alpha) - g(\alpha)| d\mu(\alpha) = \int_\Omega 1 \cdot |f(\alpha) - g(\alpha)| d\mu(\alpha) \leq \|1\|_2 \cdot \|f - g\|_2 = \|f - g\|_2,$$

where in the second inequality we used the Cauchy-Schwarz inequality. Thus, we proved (11a).

For $h \in L^2 \cap L^1$, let $\tilde{h} := h - \mathbb{E}_\alpha[h]$. By definition, $\text{Var}(h) = \|\tilde{h}\|_2^2$ and $\sigma(h) = \|\tilde{h}\|_2$. Hence,

$$\begin{aligned} |\text{Var}(f) - \text{Var}(g)| &= \left| \mathbb{E}_\alpha[\tilde{f}^2 - \tilde{g}^2] \right| = \left| \int_\Omega (\tilde{f} - \tilde{g})(\tilde{f} + \tilde{g}) d\mu(\alpha) \right| \leq \|\tilde{f} + \tilde{g}\|_2 \cdot \|\tilde{f} - \tilde{g}\|_2 \\ &\leq (\|\tilde{f}\|_2 + \|\tilde{g}\|_2) \cdot \|\tilde{f} - \tilde{g}\|_2 = (\sigma(f) + \sigma(g)) \cdot \|f - g\|_2. \end{aligned} \quad (\text{A.1})$$

In addition, $\|\tilde{h}\|_2^2 = \text{Var}(h) = \mathbb{E}_\alpha[h^2] - \mathbb{E}_\alpha^2[h] \leq \mathbb{E}_\alpha[h^2] = \|h\|_2^2$, and so $\|\tilde{h}\|_2 \leq \|h\|_2$. Applying this inequality with $h = f - g$ to (A.1) yields (11b).

Finally, we use (11b) to prove (11c):

$$|\sigma(f) - \sigma(g)| = \left| \frac{\sigma^2(f) - \sigma^2(g)}{\sigma(f) + \sigma(g)} \right| = \frac{|\text{Var}(f) - \text{Var}(g)|}{|\sigma(f) + \sigma(g)|} \leq \frac{\sigma(f) + \sigma(g)}{\sigma(f) + \sigma(g)} \|f - g\|_2 = \|f - g\|_2.$$

Appendix B. Proof of Lemma 2

Let $\{p_n(\alpha)\}_{n=0}^\infty$ be the family of orthogonal polynomials with respect to the weight function $c(\alpha)$, and let $\{\alpha_1, \dots, \alpha_N\}$ be the roots of $p_N(\alpha)$. Denote $f_j := f(\alpha_j)$ for $j = 1, \dots, N$. Let $\Pi(\alpha) = \sum_{n=0}^{N-1} \gamma_n p_n(\alpha)$ be the interpolating polynomial of f at the quadrature points, where $\{\gamma_0, \dots, \gamma_{N-1}\}$ are some unknown coefficients. The interpolation conditions $\Pi(\alpha_j) = f_j$ for $j = 1, \dots, N$ can be written in a matrix form as

$$\mathbf{A}\boldsymbol{\gamma} = \mathbf{f}, \quad (\text{B.1})$$

where $A_{i,j} = p_{j-1}(\alpha_i)$, $\boldsymbol{\gamma} = (\gamma_0, \dots, \gamma_{N-1})^T$, and $\mathbf{f} = (f_1, \dots, f_N)^T$. We define the matrix \mathbf{B} by $B_{i,j} = w_j A_{j,i} = w_j p_{i-1}(\alpha_j)$. We claim that $\mathbf{B} = \mathbf{A}^{-1}$. Indeed, for all $1 \leq i, j \leq N$,

$$(\mathbf{B}\mathbf{A})_{i,j} = \sum_{k=1}^N B_{i,k} A_{k,j} = \sum_{k=1}^N w_k p_{i-1}(\alpha_k) p_{j-1}(\alpha_k).$$

Because the Gauss quadrature rule is exact for polynomials of degree $\leq 2N - 1$ [28], $\sum_{k=1}^N w_k p_{i-1}(\alpha_k) p_{j-1}(\alpha_k) = \int_{\Omega} p_{i-1}(\alpha) p_{j-1}(\alpha) c(\alpha) d\alpha = \delta_{i,j}$, where the last equality is due of the orthogonality of p_{i-1} and p_{j-1} . By (B.1),

$$\gamma_n = (A^{-1}\mathbf{f})_{n+1} = \sum_{k=1}^N B_{n+1,k} \mathbf{f}_k = \sum_{k=1}^N w_k p_n(\alpha_k) f_k, \quad n = 0, 1, \dots, N-1.$$

Hence $\Pi(\alpha) = \sum_{n=0}^{N-1} \left(\sum_{k=1}^N w_k p_n(\alpha_k) f(\alpha_k) \right) p_n(\alpha) = f_N^{\text{gpc}}(\alpha)$, see (9) and (10).

Appendix C. An alternative to Corollary 2

We prove a slightly different bound than that of Corollary 2:

Corollary 4. *Consider a uniform grid $\alpha_1 = \alpha_{\min} < \alpha_1 \dots < \alpha_N = \alpha_{\max}$, where $\alpha_{i+1} - \alpha_i = h$ for all $i = 1, \dots, N-1$, and let $f_N^{\text{spline}} = f_N^{\text{spline}}(\alpha; f_1, \dots, f_N)$ be either the natural cubic spline, the clamped cubic spline, or the “not-a-knot” interpolating spline. Then*

$$\max_{\alpha \notin (\alpha_{i-k}, \alpha_{i+k})} \left| \frac{\partial f_N^{\text{spline}}(\alpha; f_1, \dots, f_N)}{\partial f_i} \right| \leq C \delta^k, \quad 1 < i < N, \quad 1 \leq k \leq N.$$

For the case of the natural cubic spline, $C \leq 140$ and $\delta < 0.27$.

Proof. Define the B-splines on the uniform grid by [37]

$$B_i(\alpha) := \frac{1}{h^3} \begin{cases} (\alpha - \alpha_{i-2})^3 & \text{if } \alpha \in [\alpha_{i-2}, \alpha_{i-1}] , \\ h^3 + 3h^2(\alpha - \alpha_{i-1}) + 3h(\alpha - \alpha_{i-1})^2 - 3(\alpha - \alpha_{i-1})^3 & \text{if } \alpha \in [\alpha_{i-1}, \alpha_i] , \\ h^3 + 3h^2(\alpha_{i+1} - \alpha) + 3h(\alpha_{i+1} - \alpha)^2 - 3(\alpha_{i+1} - \alpha)^3 & \text{if } \alpha \in [\alpha_i, \alpha_{i+1}] , \\ (\alpha_{i+2} - \alpha)^3 & \text{if } \alpha \in [\alpha_{i+1}, \alpha_{i+2}] , \\ 0 & \text{otherwise,} \end{cases} \quad (\text{C.1})$$

see Fig. C.8. By definition, B-splines are C^2 cubic splines. One can express any C^2 cubic spline as a linear combination of B-splines. Specifically $f_N^{\text{spline}}(\alpha) = \sum_{i=0}^{N+1} c_i B_i(\alpha)$ [37]. We first prove this for the *natural* cubic spline, for which $\frac{d}{d\alpha} f_N^{\text{spline}}(\alpha_1) = \frac{d}{d\alpha} f_N^{\text{spline}}(\alpha_N) = 0$. In this case, by (C.1), $B'_0(\alpha_1) = -B'_2(\alpha_1)$, and $B'_1(\alpha_1) = 0$. Hence,

$$0 = \frac{d}{d\alpha} f_N^{\text{gpc}}(\alpha_1) = c_0 B'_0(\alpha_1) + c_1 B'_1(\alpha_1) + c_2 B'_2(\alpha_1) = \frac{1}{h} (c_2 - c_0),$$

and so $c_0 = c_2$ and similarly $c_{N-1} = c_{N+1}$. Therefore, $f_N^{\text{spline}}(\alpha) = \sum_{i=1}^N c_i B_i(\alpha) + c_2 B_0(\alpha) + c_{N+1} B_{N+1}(\alpha)$. The interpolation conditions $f_N^{\text{spline}}(\alpha_j) = f(\alpha_j)$ for $1 \leq j \leq N$ can now be

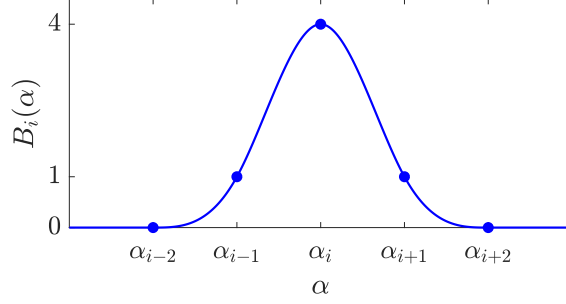


Figure C.8: The B-spline $B_i(\alpha)$, see (C.1).

written in a matrix form $\mathcal{B}\mathbf{c} = \mathbf{f}$, where $\mathbf{c} = (c_1, \dots, c_N)^T$, $\mathbf{f} = (f(\alpha_1), \dots, f(\alpha_N))^T$, and

$$\mathcal{B} = \begin{pmatrix} B_1(\alpha_1) & B_0(\alpha_1) + B_2(\alpha_1) & 0 & \dots & \dots & 0 \\ B_1(\alpha_2) & B_2(\alpha_2) & B_3(\alpha_2) & 0 & \dots & \dots \\ 0 & B_2(\alpha_3) & B_3(\alpha_3) & B_4(\alpha_3) & \dots & \dots \\ \vdots & \vdots & \vdots & \ddots & \vdots & \vdots \\ \vdots & \vdots & \vdots & \vdots & \ddots & \vdots \\ 0 & \dots & \dots & \dots & B_{N-1}(\alpha_N) + B_{N+1}(\alpha_N) & B_N(\alpha_N) \end{pmatrix}$$

Since $B_i(\alpha_i) = 4$, $B_i(\alpha_{i-1}) = B_i(\alpha_{i+1}) = 1$, and $B_i(\alpha_n) = 0$ for $|n - i| > 1$, we have that

$$\mathcal{B} = \begin{pmatrix} 4 & 2 & 0 & \dots & \dots & 0 \\ 1 & 4 & 1 & 0 & \dots & 0 \\ 0 & 1 & 4 & 1 & \dots & 0 \\ \vdots & \vdots & \vdots & \ddots & \vdots & \vdots \\ \vdots & \vdots & \vdots & \vdots & \ddots & \vdots \\ 0 & \dots & \dots & \dots & 2 & 4 \end{pmatrix}. \quad (\text{C.2})$$

By the uniqueness of the natural cubic spline [37], \mathbf{c} is unique and so \mathcal{B} is invertible and $\mathbf{c} = \mathcal{B}^{-1}\mathbf{f}$. Therefore

$$f_N^{\text{spline}}(\alpha) = \mathbf{b}(\alpha)\mathcal{B}^{-1}\mathbf{f}, \quad (\text{C.3})$$

where $\mathbf{b}(\alpha) = (B_1(\alpha), B_0(\alpha) + B_2(\alpha), B_3(\alpha), \dots, B_{N-2}(\alpha), B_{N-1}(\alpha) + B_{N+1}(\alpha), B_N(\alpha))$.

Let $\alpha \in [\alpha_{n-1}, \alpha_n]$ for some $1 < n \leq N$. By (C.3),

$$\frac{\partial f_N^{\text{spline}}(\alpha)}{\partial f_i} = (\mathbf{b}(\alpha)\mathcal{B}^{-1})_i = \sum_{\ell=1}^N (\mathbf{b}(\alpha))_{\ell} (\mathcal{B}^{-1})_{\ell,i}. \quad (\text{C.4})$$

To bound the elements of \mathcal{B}^{-1} , we recall

Theorem 4 (Demko, Moss and Smith [53]). *Let A be an invertible, positive-definite, m banded matrix. Then*

$$|A_{i,n}^{-1}| \leq C\delta^{|i-n|},$$

where

$$C = \max \left(\frac{1}{c_{\min}}, \frac{(1 + \sqrt{q})^2}{2c_{\max}} \right), \quad \delta = \left(\frac{\sqrt{q} - 1}{\sqrt{q} + 1} \right)^{\frac{2}{m}}, \quad q = \frac{c_{\max}}{c_{\min}},$$

and c_{\min} and c_{\max} are the minimal and maximal eigenvalues of A , respectively.

The matrix \mathcal{B} , see (C.2), is invertible and banded with $m = 2$. Since \mathcal{B} is strongly diagonally dominated (SDD), it is also positive-definite. Thus, \mathcal{B} satisfies the requirements of Theorem 4. Therefore, $(\mathcal{B})_{i,\ell} \leq C\delta^{|i-\ell|}$. Hence, by (C.4),

$$\left| \frac{\partial f_N^{\text{spline}}(\alpha)}{\partial f_i} \right| \leq \sum_{\ell=1}^N |(\mathbf{b}(\alpha))_\ell| C\delta^{|\ell-i|}.$$

Next, we show that $0 < \delta < 1$ by applying Gershgorin's Circle Theorem

Theorem 5 ([54]). *Let A be a rectangular matrix. Denote by D_i the closed disc in the complex plane centered at $A_{i,i}$ and with radius $R_i := \sum_{k \neq i} |A_{i,k}|$. Then every eigenvalue of A lies inside one of the discs D_i .*

In the case where $A = \mathcal{B}$, we have $R_i = 2$ and $\mathcal{B}_{i,i} = 4$ for all $1 \leq i \leq N$. Because \mathcal{B} is positive definite, its eigenvalues are real and bounded between 2 and 6; in particular, $2 \leq c_{\min}, c_{\max} \leq 6$. Hence, by Theorem 4, it follows that $\delta \leq \left(\frac{\sqrt{3}-1}{\sqrt{3}+1} \right)^{\frac{2}{2}} \approx 0.27$, and similarly $C \leq 0.65$.

Because the support of each $B_\ell(\alpha)$ is $[\alpha_{\ell-2}, \alpha_{\ell+2}]$, see Fig. C.8, then $(\mathbf{b}(\alpha))_\ell \neq 0$ only for $\ell = n-2, n-1, n$, and $n+1$. By (C.1), $0 < B_\ell(\alpha) \leq 4$ for all ℓ .

Let us consider the case where $5 \leq n \leq N-3$.²² Then

$$\left| \frac{\partial f_N^{\text{spline}}(\alpha)}{\partial f_i} \right| \leq \sum_{\ell=n-2}^{n+1} |(\mathbf{b}(\alpha))_\ell| C\delta^{|\ell-i|} \leq \sum_{\ell=n-2}^{n+1} 4 \cdot C\delta^{|\ell-i|} \leq 4 \cdot 4 \cdot C\delta^{-2}\delta^{|n-i|},$$

Taking $k = |n-i|$, one has that

$$\max_{\alpha \notin (\alpha_{i-k}, \alpha_{i+k})} \left| \frac{\partial f_N^{\text{spline}}(\alpha)}{\partial f_i} \right| \leq \tilde{C}\delta^k,$$

where $\tilde{C} = 16C\lambda^{-2} \leq 16 \cdot 0.65\lambda^{-2} \leq 140$, which completes the proof. \square

A similar proof holds for the “not-a-knot” and the clamped boundary conditions. For example, in the “not-a-knot” interpolation, $\lim_{\alpha \rightarrow \alpha_j^-} \frac{d^3}{d\alpha^3} f_N^{\text{spline}} = \lim_{\alpha \rightarrow \alpha_j^+} \frac{d^3}{d\alpha^3} f_N^{\text{spline}}$ for $j = 2, N-1$. By direct computation, see (C.1), this yields $c_0 - 4c_1 + 6c_2 - 4c_3 + c_4 = 0$. As in the above proof, we take $c_0 = 4c_1 - 6c_2 + 4c_3 - c_4$, and similarly $c_{N+1} = 4c_N - 6c_{N-1} + 4c_{N-2} - c_{N-3}$,

²²The proof for other values of n is similar.

and obtain a slightly different \mathcal{B} matrix,

$$\mathcal{B}^{\text{not-a-knot}} = \begin{pmatrix} 8 & -5 & 4 & -1 & \cdots & 0 \\ 1 & 4 & 1 & 0 & \cdots & 0 \\ 0 & 1 & 4 & 1 & \cdots & 0 \\ \vdots & \vdots & \vdots & \ddots & \vdots & \vdots \\ \vdots & \vdots & \vdots & 1 & 4 & 1 \\ 0 & \cdots & -1 & 4 & -5 & 8 \end{pmatrix}.$$

This matrix is still banded, and because its symmetric part $\frac{1}{2}(\mathcal{B} + \mathcal{B}^T)$ is diagonally dominant, it is also positive definite [55]. Therefore, the proof follows in a similar manner.

Remark. In the case of a *nonuniform grid*, the definition of the B-splines slightly changes, and so does the matrix \mathcal{B} , see (C.2). Nevertheless, \mathcal{B} remains regular and banded with $m = 2$. Therefore, Theorem 4 applies and the proof remains essentially the same.

Appendix D. Proof of Lemma 3

When f is strictly increasing, its CDF is given by

$$P(y) = \int_{\alpha_{\min}}^{f^{-1}(y)} c(\alpha) d\alpha.$$

By the Leibniz rule and the inverse function theorem,

$$p(y) = \frac{dP(y)}{dy} = c(f^{-1}(y)) (f^{-1})' = c(f^{-1}(y)) \frac{1}{f'(f^{-1}(y))}.$$

Similarly, if f is monotonically decreasing, then $P(y) = \int_{f^{-1}(y)}^{\alpha_{\max}} c(\alpha) d\alpha$, and so

$$p(y) = - \frac{c(f^{-1}(y))}{f'(f^{-1}(y))}.$$

Finally, if f is piecewise monotonic, we apply this method separately on each sub-interval on which it is monotonic, and sum up the contributions.

Appendix E. Sample MATLAB code for Algorithm 2

The following MATLAB code generates the dashed curve in Fig. 2(b).

```

1 alpha_min = -1; alpha_max = 1; N = 18; %sample size
2 f = @(x) tanh(9*x) + x/2;
3 %define the initial sample on the grid [alpha_1, ..., alpha_N]
4 samplingGrid = linspace(alpha_min, alpha_max, N);
5 samples = f(samplingGrid); % step 1
6 %define the refined sample grid [tilde_alpha_1, ..., tilde_alpha_M]
```



```

7 M = 2e6;
8 denseGrid = linspace(alpha_min, alpha_max, M);
9 fN_spline = spline(samplingGrid, samples, denseGrid); % steps 2+3
10 %When f is given explicitly, the optimal number of bins (L)
11 %is given by (14)
12 Cf = 1.69; L = Cf * M^(1/3);
13 %step 4 - histogram of fN on denseGrid, not normalized
14 [histogram, binsEdges] = hist(fN_spline, L);
15 binWidth = (max(binsEdges) - min(binsEdges)) / L;
16 %normalize the histogram so that it would be a PDF
17 pdf = histogram / (sum(histogram) * binWidth);
18 plot(binsEdges, pdf)

```

Appendix F. Proof of Theorem 3

Without loss of generality, we can assume that $f'(\alpha) \geq a > 0$. For brevity, denote $s(\alpha) = f_N^{\text{spline}}(\alpha)$, $h = h_{\max}$, and $\|f^{(4)}\|_{\infty} = \|f^{(4)}\|_{L^{\infty}[\alpha_{\min}, \alpha_{\max}]}$. In general, $s(\alpha)$ can be non-monotone. By Theorem 3, however, $|s'(\alpha) - f'(\alpha)| < C_{\text{spl}}^{(1)} \|f^{(4)}\|_{\infty} h^3$. Hence

$$s'(\alpha) \geq \frac{a}{2} > 0, \quad N > \sqrt[3]{\frac{2C_{\text{spl}}^{(1)} \|f^{(4)}\|_{\infty}}{a}} (\alpha_{\max} - \alpha_{\min}), \quad (\text{F.1})$$

and so $s(\alpha)$ is monotonically increasing and invertible for sufficiently large N .²³ Because $s(\alpha)$ interpolates $f(\alpha)$, and because both functions are monotone, then $\text{range}(s) = \text{range}(f)$. By Lemma 3, since $s, f \in C^1$ and are invertible,

$$\|p - \tilde{p}\|_1 := \int_{f(\alpha_{\min})}^{f(\alpha_{\max})} |p(y) - \tilde{p}(y)| dy = \int_{f(\alpha_{\min})}^{f(\alpha_{\max})} \left| \frac{c(f^{-1}(y))}{f'(f^{-1}(y))} - \frac{c(s^{-1}(y))}{s'(s^{-1}(y))} \right| dy. \quad (\text{F.2})$$

Denote $y = f(\alpha)$ and $\alpha_{\star} := \alpha_{\star}(\alpha) = s^{-1}(f(\alpha))$. Then by a change of variable

$$\|p - \tilde{p}\|_1 = \int_{\alpha_{\min}}^{\alpha_{\max}} \left| \frac{c(\alpha)}{f'(\alpha)} - \frac{c(\alpha_{\star})}{s'(\alpha_{\star})} \right| f'(\alpha) d\alpha = \int_{\alpha_{\min}}^{\alpha_{\max}} |s'(\alpha_{\star})c(\alpha) - f'(\alpha)c(\alpha_{\star})| \frac{1}{s'(\alpha_{\star})} d\alpha. \quad (\text{F.3})$$

For all $\alpha \in [\alpha_{\min}, \alpha_{\max}]$,

$$|s'(\alpha_{\star})c(\alpha) - f'(\alpha)c(\alpha_{\star})| \leq c(\alpha)|s'(\alpha_{\star}) - s'(\alpha)| + c(\alpha)|s'(\alpha) - f'(\alpha)| + f'(\alpha)|c(\alpha) - c(\alpha_{\star})|.$$

Because $s'(\alpha)$ and $c(\alpha)$ are differentiable,

$$|s'(\alpha_{\star})c(\alpha) - f'(\alpha)c(\alpha_{\star})| \leq D|\alpha - \alpha_{\star}| + \|c\|_{\infty}|f'(\alpha) - s'(\alpha)|, \quad (\text{F.4})$$

²³In the toy example (16), this lower bound is roughly $N > 30$.

where $D = [\|c\|_\infty \cdot \|s''\|_\infty + \|c'\|_\infty \cdot \|f\|_\infty]$.²⁴ By Lagrange's mean-value theorem, there exists β between α and α_\star such that

$$s(\alpha) - s(\alpha_\star) = s'(\beta)(\alpha - \alpha_\star).$$

On the other hand, since $\alpha_\star = s^{-1}(f(\alpha))$, then $s(\alpha_\star) = f(\alpha)$, and so

$$s(\alpha) - s(\alpha_\star) = s(\alpha) - f(\alpha).$$

Therefore $\alpha - \alpha_\star = \frac{s(\alpha) - f(\alpha)}{s'(\beta)}$. By (F.1), $s'(\beta) \geq \frac{a}{2}$, and by Theorem 1, we have $|f(\alpha) - s(\alpha)| \leq C_{\text{spl}}^{(0)} \|f^{(4)}\|_\infty h^4$. Hence,

$$|\alpha - \alpha_\star| \leq \frac{2C_{\text{spl}}^{(0)} \|f^{(4)}\|_\infty h^4}{a}.$$

By Theorem 1, $|f'(\alpha) - s'(\alpha)| \leq C_{\text{spl}}^{(1)} \|f^{(4)}\|_\infty h^3$. Hence (F.4) reads

$$|s'(\alpha_\star)c(\alpha) - f'(\alpha)c(\alpha_\star)| \leq K_1 h^3 + K_2 h^4, \quad (\text{F.5})$$

where $K_1 = C_{\text{spl}}^{(0)} \|c\|_\infty \|f^{(4)}\|_\infty$ and $K_2 = \frac{2}{a} C_{\text{spl}}^{(0)} \|f^{(4)}\|_\infty D$. Substituting $\frac{1}{s'(\alpha_\star)} \leq \frac{2}{a}$, see (F.1), and (F.5) in (F.3), for sufficiently large N such that $h = \frac{\alpha_{\max} - \alpha_{\min}}{N-1} < 1$ we have that

$$\|p - \tilde{p}\|_1 \leq \int_{\alpha_{\min}}^{\alpha_{\max}} \frac{2(K_1 + K_2)}{a} h^3 d\alpha = \frac{2(K_1 + K_2)}{a} (\alpha_{\max} - \alpha_{\min}) h^3 \leq \frac{K}{N^3},$$

where $K = \frac{2(K_1 + K_2)}{a} (\alpha_{\max} - \alpha_{\min})^4$.

Remark. If $f'(\alpha) = 0$ for some values of α , the approximation \tilde{p} is not guaranteed to converge in the L^1 norm. By (F.5), however, we can guarantee a cubic convergence for the pointwise error $p(y) - \tilde{p}(y)$, for every real number y such that $f'(\alpha)$ does not vanish on $\{\alpha \mid f(\alpha) = y\}$.

Appendix G. Proof of Lemma 4

Similarly to the proof of (F.4),

$$|s'(\alpha_\star)c(\alpha) - f'(\alpha)c(\alpha_\star)| \leq D|\alpha - \alpha_\star| + c(\alpha)|f'(\alpha) - s'(\alpha)|.$$

Because $|\alpha - \alpha_\star| \leq K_2 h^4$, then by (F.3),

$$\|p - \tilde{p}\|_1 \leq \frac{2K_2}{a} h^4 + \int_{\alpha_{\min}}^{\alpha_{\max}} |f'(\alpha) - s'(\alpha)| c(\alpha) d\alpha. \quad (\text{G.1})$$

²⁴By the same argument as (F.1), for a fixed $\epsilon > 0$ there exists a sufficiently large N_0 such that $s''(\alpha) \leq f''(\alpha) + \epsilon$ for all $N > N_0$. Therefore $\max \|s''\|_\infty \leq \max \|f''\|_\infty + \epsilon$, and so D is independent of N , and depends only on $f(\alpha)$, $c(\alpha)$, α_{\min} and α_{\max} .

Since $f'(\alpha) - s'(\alpha)$ is continuous on $[\alpha_{\min}, \alpha_{\max}]$, it vanishes and changes its sign only at finitely many points, denoted by $\alpha_{\min} = \gamma_0 < \gamma_1 < \dots < \gamma_{J_N} = \alpha_{\max}$. Using integration by parts, the last integral reads

$$\begin{aligned} \int_{\alpha_{\min}}^{\alpha_{\max}} |f'(\alpha) - s'(\alpha)| c(\alpha) d\alpha &= \eta \sum_{j=1}^{J-1} (-1)^j \int_{\gamma_j}^{\gamma_{j+1}} (f'(\alpha) - s'(\alpha)) c(\alpha) d\alpha \\ &= \eta \sum_{j=1}^{J_N-1} (-1)^j \left[c(\gamma_{j+1}) (f(\gamma_{j+1}) - s(\gamma_{j+1})) - c(\gamma_j) (f(\gamma_j) - s(\gamma_j)) - \int_{\gamma_j}^{\gamma_{j+1}} (f(\alpha) - s(\alpha)) c'(\alpha) d\alpha \right], \end{aligned}$$

where $\eta = \text{sign} [f'(\alpha_{\min}) - s'(\alpha_{\min})]$. By Theorem 1,

$$|c(\gamma_j)(f(\gamma_j) - s(\gamma_j))| \leq \|c\|_{\infty} C_{\text{spl}}^{(0)} \|f^{(4)}\|_{\infty} h^4, \quad 1 \leq j \leq J_N,$$

and

$$\left| \int_{\gamma_j}^{\gamma_{j+1}} (f(\alpha) - s(\alpha)) c'(\alpha) d\alpha \right| \leq \|c'\|_{\infty} (\gamma_{j+1} - \gamma_j) C_{\text{spl}}^{(0)} \|f^{(4)}\|_{\infty} h^4, \quad 1 < j \leq J_N.$$

Substituting these bounds in (G.1) yields

$$\|p - \tilde{p}\|_1 \leq \frac{2K_2}{a} h^4 + K_3 h^4 + K_4 J_N h^4,$$

where $K_3 = \|c'\|_{\infty} |\alpha_{\max} - \alpha_{\min}| C_{\text{spl}}^{(0)} \|f^{(4)}\|_{\infty}$ and $K_4 = 2\|c\|_{\infty} C_{\text{spl}}^{(0)} \|f^{(4)}\|_{\infty}$. In the case of a uniform grid, the first two terms are $O(N^{-4})$, and the last term is $O(N^{-4} J_N)$, which completes the proof.